The Astrophysical Journal Letters, 958:L33 (16pp), 2023 December 1 https://doi.org/10.3847/2041-8213/ad096e

A Unified Picture of Short and Long Gamma-Ray Bursts from Compact Binary Mergers

Ore Gottlieb[1,2,3], Brian D. Metzger[1,3], Eliot Quataert[4], Danat Issa[2], Tia Martineau[5], Francois Foucart[5], Matthew D. Duez[6], Lawrence E. Kidder[7], Harald P. Pfeiffer[8], and Mark A. Scheel[9]
[1] Center for Computational Astrophysics, Flatiron Institute, New York, NY 10010, USA; ogottlieb@flatironinstitute.org
[2] Center for Interdisciplinary Exploration & Research in Astrophysics (CIERA), Physics & Astronomy, Northwestern University, Evanston, IL 60202, USA
[3] Department of Physics and Columbia Astrophysics Laboratory, Columbia University, Pupin Hall, New York, NY 10027, USA
[4] Department of Astrophysical Sciences, Princeton University, Princeton, NJ 08544, USA
[5] Department of Physics and Astronomy, University of New Hampshire, 9 Library Way, Durham, NH 03824, USA
[6] Department of Physics & Astronomy, Washington State University, Pullman, WA 99164, USA
[7] Cornell Center for Astrophysics and Planetary Science, Cornell University, Ithaca, NY 14853, USA
[8] Max Planck Institute for Gravitational Physics (Albert Einstein Institute), D-14467 Potsdam, Germany
[9] TAPIR, Walter Burke Institute for Theoretical Physics, MC 350-17, California Institute of Technology, Pasadena, CA 91125, USA
Received 2023 August 31; revised 2023 November 1; accepted 2023 November 3; published 2023 November 29

Abstract

The recent detections of the ∼10 s long γ-ray bursts (GRBs) 211211A and 230307A followed by softer temporally extended emission (EE) and kilonovae point to a new GRB class. Using state-of-the-art first-principles simulations, we introduce a unifying theoretical framework that connects binary neutron star (BNS) and black hole–NS (BH–NS) merger populations with the fundamental physics governing compact binary GRBs (cbGRBs). For binaries with large total masses, $M_{\rm tot} \gtrsim 2.8\,M_{\odot}$, the compact remnant created by the merger promptly collapses into a BH surrounded by an accretion disk. The duration of the pre-magnetically arrested disk (MAD) phase sets the duration of the roughly constant power cbGRB and could be influenced by the disk mass, M_d. We show that massive disks ($M_d \gtrsim 0.1\,M_{\odot}$), which form for large binary mass ratios $q \gtrsim 1.2$ in BNS or $q \lesssim 3$ in BH–NS mergers, inevitably produce 211211A-like long cbGRBs. Once the disk becomes MAD, the jet power drops with the mass accretion rate as $\dot{M} \sim t^{-2}$, establishing the EE decay. Two scenarios are plausible for short cbGRBs. They can be powered by BHs with less massive disks, which form for other q values. Alternatively, for binaries with $M_{\rm tot} \lesssim 2.8\,M_{\odot}$, mergers should go through a hypermassive NS (HMNS) phase, as inferred for GW170817. Magnetized outflows from such HMNSs, which typically live for $\lesssim$1 s, offer an alternative progenitor for short cbGRBs. The first scenario is challenged by the bimodal GRB duration distribution and the fact that the Galactic BNS population peaks at sufficiently low masses that most mergers should go through an HMNS phase.

Unified Astronomy Thesaurus concepts: Gamma-ray bursts (629); Stellar mergers (2157); Astrophysical black holes (98); Black holes (162); Neutron stars (1108); Jets (870); Relativistic jets (1390)

1. Introduction

γ-ray bursts (GRBs) can originate from at least two distinct astrophysical systems: the collapse of massive rotating stars ("collapsars"; Woosley 1993; MacFadyen & Woosley 1999) and compact binary mergers (Eichler et al. 1989; Paczynski 1991). These two event classes are commonly associated with long GRBs (lGRBs) and short GRBs (sGRBs), respectively. Their durations follow lognormal distributions, with mean values of ∼30 s for lGRBs and ∼0.5 s for sGRBs (Kouveliotou et al. 1993; McBreen et al. 1994). The overlap of the two distributions poses a challenge to a clear distinction between the classes (Bromberg et al. 2013), particularly for bursts lasting between ∼1 and ∼30 s (Nakar 2007). A more accurate burst classification can be obtained when the GRB is followed by optical emission from the astrophysical site: a supernova Ic-BL (Galama et al. 1998; Hjorth et al. 2003) or a kilonova from a compact object merger (Li & Paczyński 1998; Metzger et al. 2010; Tanvir et al. 2013). Being the most luminous events in the sky, GRBs are detected out to large distances and, in part because of their bright synchrotron afterglows, are infrequently accompanied by detectable thermal optical counterparts.

The recent detection of optical/infrared kilonova signals following two ∼10 s long bursts in GRB 211211A (Rastinejad et al. 2022; Troja et al. 2022; Yang et al. 2022; Zhang et al. 2022) and GRB 230307A (Levan et al. 2023a; Sun et al. 2023; Yang et al. 2023) has reignited interest in the origin of long-duration GRBs that are not associated with collapsars (see also Della Valle et al. 2006; Gal-Yam et al. 2006; Bromberg et al. 2013; Lü et al. 2022; Levan et al. 2023b) but likely originating from compact binary mergers (cbGRBs). Such long durations would at least naively be unexpected in binary mergers insofar as the accretion timescales responsible for the jet launching are expected to be of the order of seconds (e.g., Narayan et al. 1992). The long-duration cbGRB (lbGRBs) events may constitute a third type of GRB population. Indeed, a closer examination of the GRB duration distribution reveals that it is best fit with three lognormal distributions (Horváth & Tóth 2016; Tarnopolski 2016). These distributions potentially correspond to three distinct populations: (i) collapsar lGRBs with $T_{90} \gtrsim 30$ s, (ii) short-duration cbGRBs (sbGRBs) from binary mergers with $T_{90} \lesssim 1$ s, and (iii) lbGRBs 211211A and GRB 230307A-like events from binary mergers, lasting $T_{90} \sim 10$ s. Below, we adhere to the conventional assumption that sbGRBs are more common than lbGRBs (Yin et al. 2023). However, we note that three lognormal distribution fits suggest otherwise (Horváth & Tóth 2016), so we do not consider the rates to be a stringent constraint.

It is tempting to associate the two cbGRB classes with the two types of compact binary mergers: black hole (BH) and neutron star (NS) and binary NS (BNS) systems. Based on the two BH–NS mergers detected during the LVK O3b run, the BH–NS merger rate was constrained to be $\mathscr{R}_{\rm BHNS} = 45^{+75}_{-33}\,{\rm Gpc^{-3}\,yr^{-1}}$ if these two events are representative of the entire population versus $\mathscr{R}_{\rm BHNS} = 130^{+112}_{-69}\,{\rm Gpc^{-3}\,yr^{-1}}$ for a broader BH–NS population (Abbott et al. 2020). In comparison, the rate of BNS mergers was found to be $\mathscr{R}_{\rm BNS} = 320^{+490}_{-240}\,{\rm Gpc^{-3}\,yr^{-1}}$ (Abbott et al. 2021). Therefore, if the two detected BH–NS events are representative, BH–NS mergers are likely to be significantly rarer than BNS mergers, similar to the scarcity of lbGRBs compared to sbGRBs. In the case of a broader BH–NS population, other merger properties, such as larger mass ratios, significant spin–orbital misalignment, and low BH spins, need to be considered (Belczynski et al. 2008), all of which would result in less massive disks and the associated challenges in launching a relativistic jet (e.g., Kyutoku et al. 2015). Regardless of the BH–NS merger rate, the fraction of this population that yields electromagnetic emission is thus likely to be negligible compared to BNS mergers (Fragione 2021; Sarin et al. 2022; Biscoveanu et al. 2023).

The main cbGRB emission phase is often accompanied by additional light-curve components. For example, in lbGRB 211211A, the variable hard burst that lasted $\sim$10 s was preceded by an oscillating precursor flare (Xiao et al. 2022) and followed by a smoother and softer γ/X-ray emission for $\sim$100 s (Gompertz et al. 2023), referred to as the "extended emission" (EE; Norris & Bonnell 2006; Perley et al. 2009). The prolonged EE, which accompanies the main signal in $\sim$25%–75% of cbGRBs (Norris & Gehrels 2008; Norris et al. 2010; Kisaka et al. 2017), is generally characterized by two components: an initial roughly flat "hump" (Mangano et al. 2007; Perley et al. 2009) followed by a power-law decay $\sim t^{-2}$ (Giblin et al. 2002; Kaneko et al. 2015; Lien et al. 2016). Any cbGRB model linked to the underlying physics of binary mergers must therefore explain the entire emission signal, including precursor flares and EE phases.

One of the main uncertainties in cbGRB models is the origin of the relativistic jets. They can be generated either through electromagnetic processes from a rotating BH (Blandford & Znajek 1977, hereafter BZ) or a magnetized NS (e.g., Goldreich & Julian 1969; Duncan & Thompson 1992; Usov 1992; Thompson 1994; Metzger et al. 2011) or hydrodynamically by the pair plasma produced by the annihilation of neutrinos emitted from the accretion disk along the polar accretion funnel (e.g., Eichler et al. 1989; Paczynski 1990; Woosley 1993; MacFadyen & Woosley 1999). Despite significant progress following the multimessenger and multiwavelength event of GW170817 (see Nakar 2020; Margutti & Chornock 2021, for reviews) and numerous advanced first-principles simulations of BNS and BH–NS mergers (e.g., Rosswog et al. 2003; Shibata et al. 2006; Rezzolla et al. 2011; Etienne et al. 2012; Hotokezaka et al. 2013b; Nagakura et al. 2014; Kiuchi et al. 2015a, 2015b, 2023; Paschalidis et al. 2015; Kawamura et al. 2016; Ruiz et al. 2016, 2018, 2020; Ciolfi et al. 2017, 2019; Ciolfi 2020; Mösta et al. 2020; Hayashi et al. 2022, 2023; Sun et al. 2022; Gottlieb et al. 2023a; Aguilera-Miret et al. 2023; Combi & Siegel 2023), the connection between the central engine and the aforementioned observed characteristics remains poorly understood.

In this paper, we review recent first-principles simulations and how they constrain the origins of the different types and phases of cbGRB light curves. In particular, we present a framework for connecting the binary merger population with the entire spectrum of cbGRB observations, which provides a first-principles explanation for the origin of the constant power prompt emission and decaying EE. The paper is structured as follows. In Section 2, we argue that while lGRB jets are powered by magnetically arrested disks (MADs), BH-powered cbGRB jets are generated before the disk enters a MAD state. In Section 3, we show that the formation of a massive disk ($M_d \approx 0.1\,M_\odot$) around the postmerger BH inevitably powers lbGRBs such as GRB 211211A. In Section 4, we present two self-consistent models as the origin of sbGRBs, prompt-collapse BHs forming low-mass disks and hypermassive NSs (HMNSs), and we describe why we favor these two scenarios over the alternatives, such as delayed-collapse BHs, supramassive NSs (SMNSs), white dwarf (WD) mergers/accretion-induced collapse (AIC), and neutrino-driven jets. In Section 5, we discuss the origin of the precursor and EE of cbGRBs, compare the models with observables, and deduce that sbGRBs are likely powered by HMNSs, whereas lbGRBs are powered by BHs with massive disks. We summarize and conclude in Section 6.

2. Collapsar GRBs versus CBGRBs: To Be MAD or Not to Be MAD

lGRBs and cbGRBs take place in very different astrophysical environments, leading to distinct conditions for their occurrence and potentially differing central engines that drive these events. A recent study by Gottlieb et al. (2023c) demonstrated that lGRB jets are launched from BHs once the accretion disk becomes MAD. The reason for this is that a successful jet launching requires the Alfvén velocity to surpass the freefall velocity of the inflowing gas, allowing magneto-hydrodynamic (MHD) waves to escape from the BH ergosphere and form the emerging jet (Komissarov & Barkov 2009). In other words, a sufficiently powerful magnetic flux empowers a BH to launch jets in defiance of the inward motion of the surrounding stellar envelope. Numerical simulations (Gottlieb et al. 2022a) have confirmed that this process is sustained once the disk becomes MAD, occurring when the dimensionless magnetic flux on the BH reaches a threshold of $\phi \equiv \Phi(\dot{M} r_g^2 c)^{-1/2} \approx 50$, where r_g is the BH gravitational radius, Φ is the dimensional magnetic flux, and $\dot{M}$ is the mass accretion rate (e.g., Tchekhovskoy 2015). The BZ-jet power is determined by Blandford & Znajek (1977) and Tchekhovskoy et al. (2011),

$$P_j \sim \frac{c}{r_H^2}\Phi^2 f(a), \tag{1}$$

where r_H is the radius of the BH horizon, and $f(a)$ is the functional dependency on the BH spin. This relation can also be expressed in terms of the dimensionless magnetic flux ϕ,

$$P_j = \dot{M}\eta_\phi \eta_a c^2, \tag{2}$$

where the jet launching efficiencies are defined as

$$\eta_\phi = \left(\frac{\phi}{50}\right)^2;\ \eta_a = (1.063a^4 + 0.395a^2), \tag{3}$$

where η_a is the maximum efficiency for a given BH spin calibrated by Lowell et al. (2023). In a MAD state, $\eta_\phi = 1$, and thus Equation (2) shows that the jet launching efficiency depends only on a. This implies that the lGRB timescale is governed either by the BH spin-down timescale, $\dot{a}$ (Jacquemin-Ide et al. 2023), or by the accretion timescale (e.g., Gottlieb et al. 2022a).

In contrast to collapsars, where the newly formed BH is embedded in a dense massive stellar core, binary mergers take place in a considerably less dense environment surrounding the central engine. Consequently, jets can emerge well before the disk reaches a MAD state at $T_{\rm MAD}$. Numerical simulations incorporating self-consistent models of binary mergers, capable of launching these jets, have verified this expectation (e.g., Hayashi et al. 2022, 2023). These simulations show that the compactness of the postmerger disk allows for the dimensional magnetic flux to rapidly accumulate on the BH,[10] resulting in a constant jet power, $P_j(t < T_{\rm MAD}) \sim \Phi \sim$ const (Equation (1)). Due to the decaying mass accretion rate, the dynamical importance of the magnetic field (as measured by the dimensionless magnetic flux $\phi \propto \Phi \dot{M}^{-1/2}$) grows with time. Once $\phi \approx 50$ is reached, the disk enters a MAD state, which saturates the jet launching efficiency $\eta_\phi \approx 1$. Thereafter, the jet power follows the declining mass accretion rate, $P_j(t > T_{\rm MAD}) \propto \dot{M}$, following Equation (2).

Unlike collapsars, the disks formed from binary mergers do not have an external supply, resulting in their steady depletion and a continuous decrease in the BH mass accretion rate. In fact, at $t \gtrsim 0.1$ s, the mass accretion rate $\dot{M}$ follows a single power-law decay without a characteristic timescale relevant to cbGRBs (which, in the collapsar case, is set by the structure of the progenitor star). This implies that, in contrast to lGRBs, where jet launching persists during the MAD phase of the disk and its timescale is set by $\dot{M}$ or $\dot{a}$, in mergers,[11] it is the MAD transition at $T_{\rm MAD}$ (dictated by M_d and Φ) that eventually causes the jet power to decay, thus setting the cbGRB duration, as we now describe.

3. lbGRBs from BHs with Massive Disks

Gottlieb et al. (2023a) presented first-principles simulations of a BH–NS merger with mass ratio $q = 2$, which results in a rapidly spinning BH with $a \simeq 0.86$. A substantial accretion disk of mass $M_d \approx 0.15\,M_\odot$ formed around the BH, resulting in a high initial accretion rate, $\dot{M} \sim M_\odot$ s^{-1}. We find a similar outcome here for five simulations of a BNS merger of component masses 1.06 and $1.78\,M_\odot$, initialized from the endpoint of the merger simulations of Foucart et al. (2023). In that system, the remnant promptly collapses to a BH with $a = 0.68$, surrounded by a disk with $M_d \approx 0.1\,M_\odot$ (see the Appendix for the full numerical results of the BNS merger simulations). Additionally, we perform five BH–NS merger simulations with component masses of 4.05 and $1.35\,M_\odot$, respectively. The BH has a premerger spin of $a \approx 0.087$. The postmerger BH has a spin of $a \approx 0.59$ and mass of $5.26\,M_\odot$ and is surrounded by a disk with $M_d \approx 0.007\,M_\odot$. Refer to the Appendix for a brief discussion of the simulation setup and time evolution of $\dot{M}$, ϕ, P_j, $\eta_a\eta_\phi$. A detailed analysis of the results will be published in future work.

Equation (2) shows that the jet power depends on both the mass accretion rate and the magnetic flux on the BH, Φ. Binary compact mergers produce small accretion disks that promptly feed the available magnetic flux onto the BH.[12] Because Φ hardly changes thereafter during the subsequent accretion phase, this results in a constant jet power $P_j \sim$ const with a magnitude that depends on the disk's poloidal field strength. This is demonstrated in Figure 1, which depicts the jet power as a function of time for different values of Φ and M_d.

If the initial plasma beta in the disk is low (leading to large Φ), then the jet launching efficiency is high, and the jet starts with too much power compared to prompt sbGRB luminosities. In such cases, the dimensionless magnetic flux on the BH quickly saturates and the disk becomes MAD, ending the constant jet power phase. This translates to a relatively short and exceedingly luminous prompt cbGRB (see, e.g., the red and black dashed lines in Figure 1). This outcome challenges the model of Gao et al. (2022), which suggests that a strong magnetic field can halt accretion to prolong the cbGRB duration.

If instead, the initial plasma beta in the disk is high (low Φ) or the initial magnetic field configuration is predominantly toroidal (see, e.g., the Appendix), then the jet launching efficiency is low, and the jet can generate a luminosity characteristic of prompt sbGRBs. Over time, the efficiency increases due to the development of a global poloidal magnetic field and the decrease in the mass accretion rate that follows[13] $\dot{M} \sim t^{-2}$, as was also found in other numerical simulations (Fernández et al. 2015, 2017, 2019b; Christie et al. 2019; Metzger & Fernández 2021; Hayashi et al. 2022), where the normalization of the mass accretion rate is set by M_d. When the disk finally becomes MAD at $T_{\rm MAD}$, the efficiency stabilizes at $\eta_\phi \approx$ const, and Equation (2) reads $P_j \sim \dot{M} \sim t^{-2}$. The two phases of $P_j(t < T_{\rm MAD}) \sim P_0$ and $P_j(t > T_{\rm MAD}) \sim t^{-2}$ are generic for BH-powered cbGRB jets. This motivates future analytic and numerical models to consider such temporal evolution of the jet power, with two free parameters: $T_{\rm MAD}$, determined by the values of ϕ, and P_0, determined by Φ.

We stress that a roughly constant jet power does not imply a constant γ-ray luminosity. First, as shown in Figure 4(d) in the Appendix, the jet power itself exhibits temporal variability, particularly for the initially toroidal configurations, owing to the stochastic nature of the dynamo process. Second, different portions of the jet undergo different levels of mixing and mass entrainment by the surrounding environment, leading to fluctuations in the baryon loading, magnetization, and Lorentz factor. These variations likely translate to a range of radiative efficiencies. This implies that even though the jet power remains roughly constant, on average (consistent with the observed lack of temporal evolution in the statistical properties of GRB light curves throughout the burst; e.g., McBreen et al. 2002), different light curves can exhibit different shapes and variability, depending on the specifics of the merger.

[10] If the disrupted NS has a purely toroidal field configuration, Φ is not constant but slowly increases due to the dynamo process.

[11] The postmerger disk mass is negligible compared to the BH mass, so no appreciable spin-down is expected in binary mergers.

[12] More massive BHs generally only lead to more compact disks (e.g., Fernández et al. 2020), making this result robust.

[13] Energy injection from alpha-particle recombination can also act to steepen the mass accretion power law after neutrino cooling is no longer important at $t \gtrsim 1$ s (Metzger et al. 2008a; Haddadi et al. 2023).

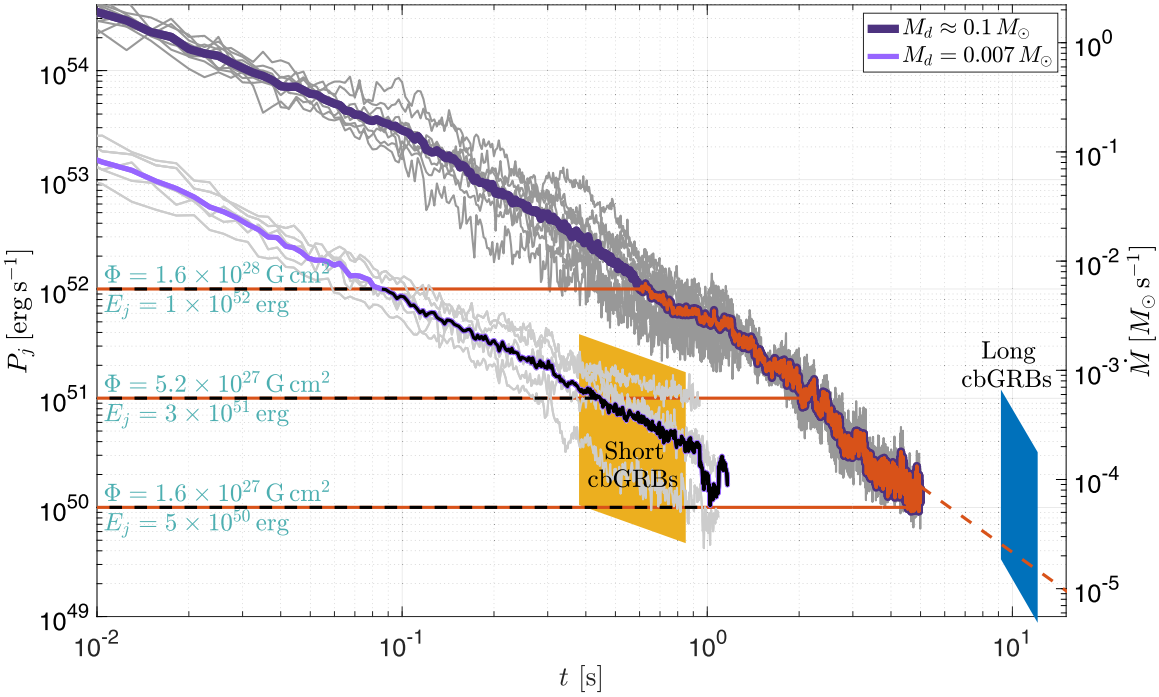

Figure 1. The jet power evolution of postmerger accretion disks for varying levels of magnetic flux ranging from non-MAD to MAD. Dark gray lines show the postmerger mass accretion rate evolution (right vertical axis) obtained for four BH–NS merger simulations (Gottlieb et al. 2023a) and the five BNS merger simulations presented here, all of which generate massive disks, $M_d \approx 0.1\ M_\odot$. Light gray lines delineate the postmerger accretion rates from five BH–NS merger simulations that result in disk masses $M_d \approx 0.007\ M_\odot$. The dark (light) purple lines mark the logarithmic averages of the mass accretion rates for $M_d \approx 0.1\ M_\odot$ ($M_d = 0.007\ M_\odot$), which constitute the maximum jet power assuming $\eta_a = 1$ corresponding to a BH spin $a \approx 0.87$ (left vertical axis). Black (for low-mass disks) and orange (for high-mass disks) lines schematically illustrate the jet power evolution for different assumptions about the dimensional magnetic flux threading the BH, Φ, and the corresponding total jet energy, E_j, for the case of the massive disk. Since the magnetic flux on the BH is likely accumulated early and hence remains nearly constant before the disk transitions to MAD, the jet power, P_j, is also predicted to be roughly constant at these times, powering the prompt emission. Once the dimensionless magnetic flux saturates in the MAD state, the jet power saturates at $P_j = \dot{M}c^2$ and thus follows the mass accretion rate $\dot{M} \propto t^{-2}$ thereafter, powering the EE (we have extrapolated P_j by a dashed line to later times). The yellow (blue) region outlines the estimated average jet power and duration T_{90} (T_{50}) of the sbGRB (lbGRB) population based on prompt emission and afterglow observations (see text). While the jets from massive disks (orange lines) are either too powerful or operate for too long, compared to the prompt sbGRB population, BH accretion from massive disks nicely matches the observed properties of prompt lbGRBs. Jets from less massive disks (black lines) fit the luminosity and duration of sbGRBs and are unable to give rise to lbGRBs (see Figures 4 and 5 for the jet power evolution in simulations).

3.1. Constraints from cbGRB Observations

To compare the predictions of numerical simulations with observational data, we need to deduce the true jet properties from observations. The observed duration of the γ-ray prompt emission from cbGRB, T_{90}, varies depending on the detectors used (Bromberg et al. 2013) and whether the GRB duration distribution is modeled assuming two (lGRBs and cbGRBs) or three (lGRBs, sbGRBs, and lbGRBs) populations. To estimate the range of T_{90} for sbGRBs, we refer to the lowest and highest T_{90} values found among two and three Gaussian fits to Fermi and BATSE duration distributions in Tarnopolski (2016) and find $0.38\ \mathrm{s} \leqslant T_{90} \leqslant 0.85\ \mathrm{s}$. For lbGRBs, we take the prompt emission durations of recent events GRB 211211A and GRB 230307A as boundaries, where $T_{50} = 12.1$ s (Tamura et al. 2021) and $T_{50} = 9.2$ s (Svinkin et al. 2023), respectively. The use of T_{50} instead of T_{90} in this case is motivated by the comparable radiated energies of the prompt burst and EE phases (Kaneko et al. 2015; Zhu et al. 2022), rendering T_{50} a more accurate estimate for the prompt duration.

The characteristic jet power of cbGRBs can be estimated as

$$P_{\rm obs} = \frac{f_b\ E_{\rm iso,\gamma}}{\epsilon_\gamma T_{90(50)}}, \tag{4}$$

where $E_{\rm iso,\gamma}$ is the isotropic equivalent γ-ray energy, f_b is the beaming fraction, and ϵ_γ is the radiative efficiency of the γ-ray emission. We take $E_{\rm iso,\gamma} \approx 2 \times 10^{51}$ erg for sbGRBs (Fong et al. 2015), while for lbGRBs, we adopt the values $E_{\rm iso,\gamma} \approx 5.3 \times 10^{51}$ erg (Yang et al. 2022) and $E_{\rm iso,\gamma} \approx 1.5 \times 10^{52}$ erg (Levan et al. 2023a) measured for GRB 211211A and GRB 230307A, respectively. We adopt a range of beaming factors, $0.01 \leqslant f_b \leqslant 0.11$ (Fong et al. 2015), corresponding to a true γ-ray jet energy for sbGRBs of $E_{\rm obs,\gamma} \approx 2 \times 10^{49}$–$2 \times 10^{50}$ erg (Fong et al. 2015). Early estimates of the γ-ray efficiency in lGRBs found $\epsilon_\gamma \approx 0.5$ (Panaitescu & Kumar 2002), but later analyses by Beniamini et al. (2015, 2016) suggested a lower value of $\epsilon_\gamma \approx 0.15$. Berger (2014) found that the ratio of cbGRB prompt to afterglow energy is higher by an order of magnitude compared to lGRBs, indicating a potentially higher ϵ_γ for cbGRBs. Nevertheless, this discrepancy might be attributed to the brighter afterglow emission arising from the denser large-scale environments surrounding the massive star progenitors of lGRBs. It thus remains unclear whether the difference between lGRBs and cbGRBs results from variations in the external medium or is intrinsic (i.e., attributed to higher ϵ_γ in cbGRBs) due to, e.g., substantial wobbling jet motion in collapsar jets (Gottlieb et al. 2022b). We thus consider a range of $0.15 \leqslant \epsilon_\gamma \leqslant 0.5$ in our estimates.

Figure 1 compares theoretical and numerical estimates of the jet power with cbGRB observations. The right vertical axis shows the characteristic evolution of the BH accretion rate as a

function of time after the merger (purple lines), which we have obtained by averaging the results of BH–NS and BNS merger simulations (gray lines), which produce massive disks with $M_d \approx 0.1\,M_\odot$ (dark purple) and $M_d = 0.007\,M_\odot$ (light purple). The jet power, displayed on the left vertical axis, is expected to be roughly constant at early times, insofar as most of the magnetic flux Φ accumulates on the BH quickly. However, as the accretion rate drops, the dimensionless magnetic flux $\phi \propto \dot{M}^{-1/2}$ increases with time until the disk enters a MAD state and the jet efficiency $\eta_\phi \approx 1$ saturates, marking the characteristic MAD timescale, which represents the end of the prompt emission phase. After this point, the jet power $P_j \approx \eta_a \dot{M} c^2$ (Equation (2)) tracks the decaying mass accretion rate $P_j \propto t^{-2}$, which, as we show in Section 5.3, represents the EE.

As mentioned in Section 3, if the initial Φ is high (red and black dashed lines), the jet is too powerful to match the characteristic power of sbGRBs (yellow region) and lbGRBs (blue region). In order to achieve that power, the magnetic flux needs to be $\Phi \sim 10^{27.5}\,\mathrm{G\,cm^2}$ (bottom orange line). For such a flux, if the disk is massive (dark purple), the accretion disk can only enter a MAD state after several seconds, significantly longer than the sbGRB duration, $T_{\rm MAD} \gg T_{90}$. On the other hand, flux at roughly this same level, $\Phi \lesssim 10^{27}\,\mathrm{G\,cm^2}$, leads to a jet that naturally achieves both the correct power and duration of the lbGRB class (blue region; see Figure 5 for the lbGRB jet power evolution in simulations). Lighter disks (light purple) can enter the MAD state on the sbGRB characteristic timescale (middle black line) to reproduce both the duration and luminosity of sbGRBs (yellow region; see Figure 5 for the sbGRB jet power evolution in simulations).

We conclude that for relatively high disk masses, $M_d \gtrsim 0.1\,M_\odot$ (consistent with that required to produce the kilonova ejecta in GW170817; e.g., Perego et al. 2017; Siegel & Metzger 2017), the resultant jets exhibit either excessively high power (if the seed magnetic flux threading the disk is large) or lower power with an extended duration of activity (if the seed flux is weaker). The former is ruled out observationally, implying that massive disks must give rise to lbGRBs. Therefore, if the jet in GW170817 was powered by a BH surrounded by a massive disk, then the inferred jet energy, $E_j \approx 10^{49}$–10^{50} erg (Mooley et al. 2018), indicates that the jet was not a luminous cbGRB but rather an lbGRB (e.g., the bottom orange line in Figure 1). Unfortunately, because the jet was $\sim 20^\circ$ off-axis (Mooley et al. 2018), the bulk of the γ-ray emission was beamed away from Earth, precluding a direct measurement of the jet duration.

3.2. Disfavored Solutions

Here we explore potential caveats to the conclusions of the previous subsection. However, finding reasons to disfavor each, we shall ultimately conclude that BHs surrounded by massive disks remain the most likely explanation for lbGRBs.

3.2.1. Lower Postmerger BH Spins

According to Equation (2), one potential way to reduce the jet power is to decrease the maximum efficiency η_a by considering a lower postmerger BH spin for an otherwise similar magnetic flux. For example, a BH spin of $a \approx 0.4$ yields a maximum efficiency of only $\eta_a \approx 0.1$ (Lowell et al. 2023). This would allow BHs with massive disks to power sbGRBs provided the BH spin obeyed $a \lesssim 0.4$. However, this requirement conflicts with the results of numerical relativity simulations, which find postmerger BH spins $0.6 \lesssim a \lesssim 0.8$ (Kiuchi et al. 2009; Kastaun & Galeazzi 2015; Sekiguchi et al. 2016; Dietrich et al. 2017) for BNS mergers, corresponding to $0.3 \lesssim \eta_a \lesssim 0.7$. BH–NS mergers result in comparable or slightly higher remnant BH spins, at least for systems leading to the formation of massive accretion disks (Foucart et al. 2011, 2013, 2014, 2017, 2019; Kyutoku et al. 2011, 2015; Kawaguchi et al. 2015). Appealing to a lower BH spin can thus only reduce the jet energy by a factor of ≈ 2 compared to our estimates assuming $\eta_a \approx 1$.

3.2.2. Delayed Jet Launching

As the magnetic field in postmerger accretion disks is anticipated to be predominantly toroidal (e.g., Ruiz et al. 2018), a jet of significant power may only be launched after a dynamo process in the disk generates a sufficiently strong global poloidal field. If the seed magnetic field is weak, the jet onset might be delayed for several seconds (see, e.g., Hayashi et al. 2023), thus operating for only a brief period before the disk transitions into a MAD state. This would make it possible for a BH with a massive disk to produce an sbGRB. Nevertheless, it is unlikely that this scenario can serve as a generic explanation for sbGRBs, as fine-tuning is required to launch the jet only briefly after ~ 10 s, just before the disk reaches a MAD state, in order to achieve $T_{90} \lesssim 1$ s.

3.2.3. Misestimating the cbGRB Duration

Another possible caveat worth exploring is whether the jet duration could be inferred incorrectly from observations. Such an erroneous estimation could occur while (i) converting from the engine activity duration to T_{90} or (ii) due to uncertainties in observations.

(i) If the interaction of the jet with the external medium is sufficiently strong to decelerate the jet head to subrelativistic velocities, the radial extent of the jet can become significantly shorter than $T_{\rm MAD}/c$, leading to an observed GRB duration considerably shorter than the MAD timescale over which the jet is launched. However, for the typical properties of merger ejecta and cbGRB jet energies, the jet head exhibits at least mildly relativistic motion from the onset (Gottlieb & Nakar 2022), supporting the usual assumption that the GRB duration follows the activity time of the jet (i.e., $T_{90} \sim T_{\rm MAD}$).

(ii) In collapsars, the physics of jet propagation (Bromberg et al. 2011) and the observed GRB duration distribution (Bromberg et al. 2012) support a substantial fraction of jets being choked inside the star (see also Gottlieb et al. 2022a). Some jets may operate just long enough to break out of the star and power a short-duration GRB (Ahumada et al. 2021; Rossi et al. 2022). If collapsar jets outnumber those originating from binary mergers within the sGRB population, this could, in principle, lead to underestimates of the typical duration of binary merger jets. However, while such an increase in the inferred T_{90} of binary merger jets could potentially alleviate the tension in accounting for sbGRBs from massive BH disks, it provides no natural explanation for the bimodal distribution of GRB durations.

4. Origin of Prompt cbGRBs

While we conclude that massive disks likely produce lbGRBs, Equation (2) shows that sbGRBs could instead emerge naturally from less massive BH disks. To explore whether variations in the disk mass from different merger outcomes are compatible with such a scenario, we now review the outcomes of compact binary mergers, as predicted by numerical relativity simulations of BNS (Rezzolla et al. 2010; Hotokezaka et al. 2011, 2013a; Sekiguchi et al. 2011; Giacomazzo & Perna 2013; Kiuchi et al. 2014, 2015a; Dietrich et al. 2015; Kastaun & Galeazzi 2015; Foucart et al. 2016; Kawamura et al. 2016; Sekiguchi et al. 2016; Dietrich et al. 2017; Hanauske et al. 2017; Radice et al. 2018a; Ruiz et al. 2018; Shibata & Hotokezaka 2019) and BH–NS (Shibata & Uryū 2006, 2007; Etienne et al. 2008; Rantsiou et al. 2008; Shibata & Taniguchi 2008, 2011; Duez et al. 2010; Foucart et al. 2011, 2014, 2017, 2019; Kyutoku et al. 2011, 2013; Foucart et al. 2012; Foucart 2012; Kawaguchi et al. 2015; Kyutoku et al. 2015; Hayashi et al. 2021) mergers.

4.1. Prompt-collapse BHs

When the total mass of a BNS exceeds a critical threshold, $M_{\rm tot} \gtrsim 2.8\,M_\odot$, the remnant created by the merger promptly collapses into a BH surrounded by an accretion disk (Bauswein et al. 2013), the mass of which depends sensitively on the binary mass ratio. For unequal mass ratios ($q \gtrsim 1.2$), as characterized by our BNS merger simulations, the lighter NS is disrupted, resulting in a massive accretion disk, $M_d \approx 0.1\,M_\odot$. By contrast, prompt-collapse mergers with $q \approx 1$ generate significantly smaller disk masses, $M_d \lesssim 10^{-2}\,M_\odot$ (see Shibata & Hotokezaka 2019, for a review). As the accretion rate scales linearly with the disk mass (Figure 1), if Φ is largely independent of M_d, then disk masses of $M_d \lesssim 10^{-2}\,M_\odot$ could power jets consistent with sbGRB observations. This implies that sbGRBs can, in principle, be powered through massive BNS mergers with $M_{\rm tot} \gtrsim 2.8\,M_\odot$ and $q \approx 1$. In BH–NS mergers, similarly low disk masses of $M_d \lesssim 10^{-2}\,M_\odot$ are possible for high binary mass ratios, $q \gg 1$, low premerger BH spin, or large spin–orbit misalignment (Foucart et al. 2018).

The region $M_{\rm tot} > 2.8\,M_\odot$ in Figure 2 overviews this scenario. Low disk masses, such as those produced by equal-mass BNS mergers that undergo prompt BH formation (bottom yellow region) or high mass ratio BH–NS mergers (top right yellow region),[14] give rise to sbGRBs. The opposite case of mergers forming massive BH disks then powers lbGRBs (blue region). If BHs power all cbGRB jets, then it is expected that the cbGRB duration spectrum will be continuous via the disk mass distribution. This seems to be in tension with the observed bimodal distribution. This scenario also poses an additional requirement on the rates given that most cbGRBs arise from BNS mergers. If sbGRBs are more common than lbGRBs, this would require that $q \approx 1$ BNS mergers (sbGRBs) should be more common than unequal mass ratio BNS mergers (lbGRBs). While consistent with the mass ratio distribution of the Galactic BNS population being narrowly concentrated around $q \lesssim 1.2$ (Vigna-Gómez et al. 2018; Farrow et al. 2019), this picture is in tension with the BNS masses being below the expected prompt-collapse threshold of $\approx 2.8\,M_\odot$, as we now discuss.

4.2. Long-lived HMNSs

Observations of Galactic BNSs indicate an average NS mass of $M_{\rm NS} \approx 1.33\,M_\odot$ (Özel et al. 2012; Kiziltan et al. 2013; Özel & Freire 2016; Farrow et al. 2019). If representative of the extragalactic merger population as a whole, this relatively low mass suggests that most mergers will not undergo a prompt collapse into a BH given current constraints on the NS equation of state (EoS; e.g., Margalit & Metzger 2019). Furthermore, larger Fe cores are generally expected to result in both more energetic explosions and greater NS natal kicks, resulting in a correlation between these two properties (Tauris et al. 2017). Since large kicks tend to unbind the binary, this makes less massive BNS systems more likely to eventually merge compared to their more massive counterparts.

The merger of BNS systems with $M_{\rm tot} \lesssim 2.8\,M_\odot$ results in the formation of a highly magnetized differentially rotating HMNS, which only collapses into a BH after some delay (e.g., Shibata & Taniguchi 2006; Kastaun & Galeazzi 2015; Hanauske et al. 2017). As a result of amplification of the magnetic field via differential rotational and instabilities, such HMNSs have the potential to produce energetic jets that could be the source of sbGRBs (Kluźniak & Ruderman 1998). One challenge to this scenario is that the polar outflows from HMNSs are subject to baryon contamination of $\sim 10^{-4}\ M_\odot\ {\rm sr}^{-1}$ driven by strong neutrino heating from the atmosphere just above the surface (Thompson et al. 2001; Dessart et al. 2009; Metzger et al. 2018), which, for jets of sbGRB energies, limits their bulk Lorentz factors to $\Gamma \lesssim 10$ (Metzger et al. 2008b). While relatively low, $\Gamma \sim 10$ might nevertheless be compatible with constraints based on compactness arguments in cbGRBs (Nakar 2007).[15]

Comparing the observed properties of cbGRBs with the energy output and lifetime of HMNSs is challenging due to the sensitivity of the latter to several theoretically uncertain properties of the postmerger system. The lifetime of the HMNS is governed by various physical processes, including neutrino cooling and angular momentum transport, the timescales for which in turn depend on factors such as the strength of the remnant's large-scale magnetic field, the saturation level of various MHD instabilities giving rise to turbulent transport, and the initial distribution of angular momentum and temperature (Margalit et al. 2022). The complexity of incorporating all of these physical processes into long-term simulations, on top of uncertainties in the EoS, renders the lifetimes of HMNSs highly uncertain (Hotokezaka et al. 2013a; Dietrich et al. 2017).

More massive binaries in general produce HMNSs with shorter lifetimes (Shibata & Taniguchi 2006; Bauswein et al. 2013). For binaries with $M_{\rm tot} \approx 2.7\,M_\odot$, the HMNS lifetime is primarily governed by angular momentum transport and the specific EoS (Hanauske et al. 2017). For less massive HMNSs, the collapse is dictated either by angular momentum transport with a timescale of $T_{\rm HMNS} \sim 0.1$ s or, if the HMNS is partially thermally supported (Hotokezaka et al. 2013a; Kaplan et al.

[14] Figure 2 should ideally cover the 3D space ($M_{\rm tot}$, q, a), as the final disk mass is sensitive to the component of the initial BH spin aligned with the orbital angular momentum. Larger values of the BH spin result in more massive disks, and lower values of the BH spin result in lower-mass disks (or no disks at all). Nonetheless, the figure qualitatively captures the dependence of the results on ($M_{\rm tot}$, q).

[15] While compactness arguments in sGRB 090510 imply an ultrarelativistic Lorentz factor (Ackermann et al. 2010), it was proposed that this sGRB may be a misclassified collapsar event (e.g., Panaitescu 2011).

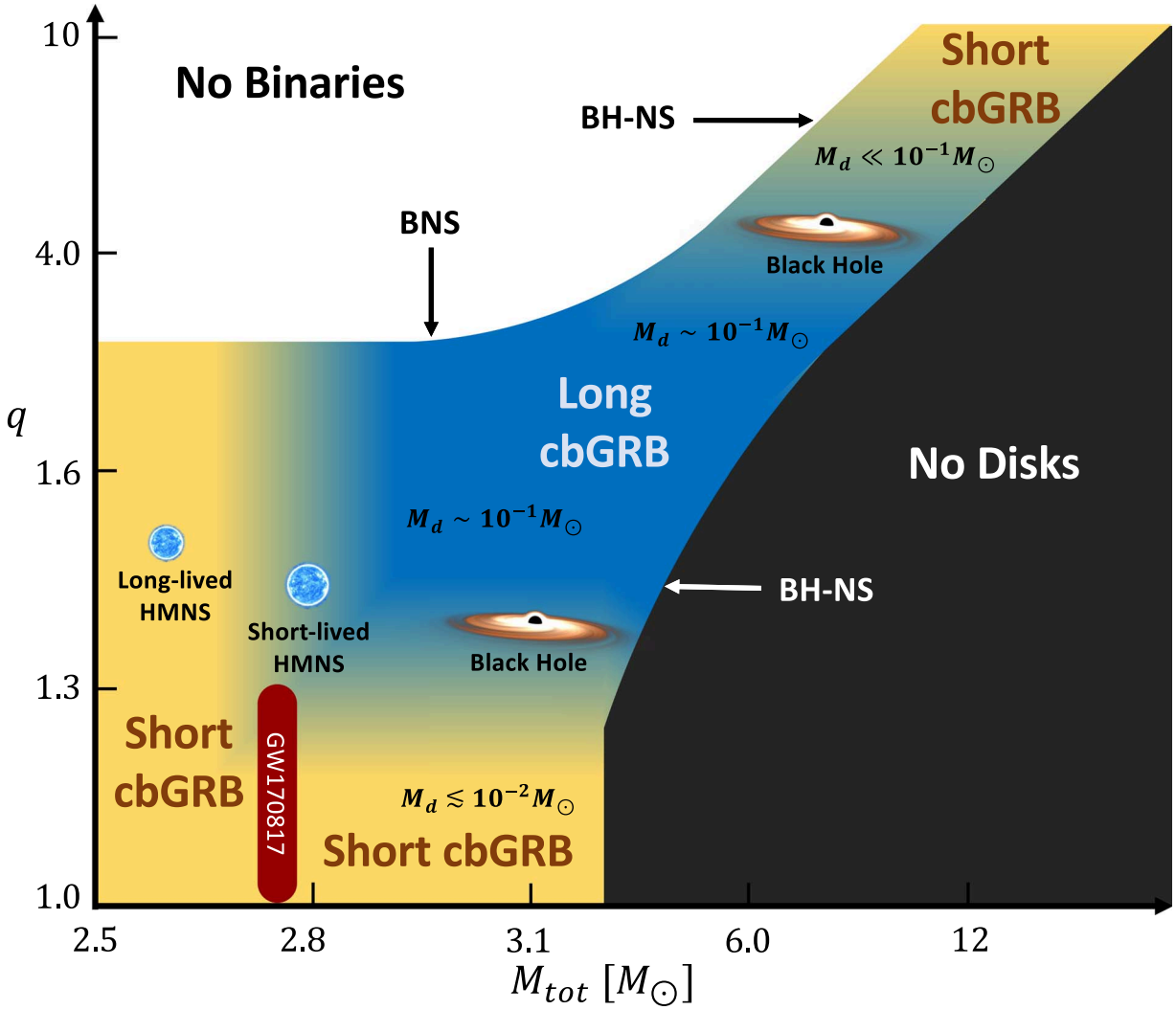

Figure 2. The outcomes of compact object mergers and their ability to power various cbGRB subclasses as a function of the binary mass ratio (vertical axis) and total mass (horizontal axis). lbGRBs occur in high-$M_{\rm tot}$ and high-q BNS mergers that form a massive BH disk of $M_d \sim 10^{-1}\,M_\odot$ or in high premerger BH spin and low mass ratio BH–NS mergers (blue region). sbGRBs may arise either from equal mass ratio BNS mergers (bottom yellow region) and low premerger BH spin/high mass ratio BH–NS mergers (top yellow region) or by HMNSs formed in BNS mergers with $M_{\rm tot} \lesssim 2.8\,M_\odot$ (left yellow region). If BH-powered jets are different than HMNS-powered jets, then the absence of evidence for distinct subclasses of sbGRBs suggests that either BHs or HMNSs are likely to be the sole origin of these events; i.e., only one of the proposed sbGRB scenarios is correct. The Galactic BNS mass distribution, the bimodal GRB duration distribution, and GW170817 observations favor HMNSs as the engine of sbGRB jets.

2014), by neutrino cooling with a timescale of $T_{\rm HMNS} \sim 1$ s (Sekiguchi et al. 2011). The binary mass ratio also plays a role, with greater asymmetry resulting in a longer HMNS lifetime due to increased angular momentum support (Dietrich et al. 2017).

Numerical simulations of $q \lesssim 1.2$ binaries with $M_{\rm tot} \gtrsim 2.7\,M_\odot$, which birth long-lived ($T_{\rm HMNS} \approx T_{90}$) HMNSs with strong magnetic fields $B \gtrsim 10^{15}$ G, found the latter capable of generating sbGRB-like emission (Ruiz et al. 2016; Ciolfi et al. 2019; Ciolfi 2020; Mösta et al. 2020; Ruiz et al. 2020; Combi & Siegel 2023; Kiuchi et al. 2023). On the other hand, Most & Quataert (2023) found for a similar magnetic field and binary mass that the jet emission is lower by several orders of magnitude compared to other simulations. Furthermore, the HMNS lifetime varies greatly among those simulations, from $T_{\rm HMNS} \sim 10$ ms to $T_{\rm HMNS} \gtrsim 1$ s, demonstrating the uncertainty in the HMNS lifetime, even when similar magnetic fields and $M_{\rm tot}$ are considered (Ruiz et al. 2016, 2020; Ciolfi et al. 2019; Ciolfi 2020; Aguilera-Miret et al. 2023; Kiuchi et al. 2023; Most & Quataert 2023). The specific properties of the binary and the EoS thus play a crucial role in determining the characteristics of HMNSs.

Perhaps the tightest constraint on the properties of HMNSs comes through the interpretation of the first multimessenger BNS system, GW170817, characterized by $M_{\rm tot} \approx 2.75\,M_\odot$ and $q \lesssim 1.3$ (Abbott et al. 2019). GW170817 provided valuable insights into the EoS of dense matter (Radice et al. 2018b) and supported the existence of a transient HMNS phase (Margalit & Metzger 2017; Shibata et al. 2017; Rezzolla et al. 2018). The large quantity of slow-moving ejecta inferred from the kilonova argues against a prompt collapse of the BH but is consistent with the expectation of disk outflows from a merger accompanied by an HMNS phase. The low inferred abundance of lanthanides in the ejecta (e.g., Kasen et al. 2017) supports strong neutrino irradiation of the disk by the HMNS (e.g., Metzger & Fernández 2014; Kasen et al. 2015; Lippuner et al. 2017). These findings thus point toward the requirement of a sufficiently stiff EoS, capable of supporting the formation of an

HMNS from the GW170817 merger with $M_{\rm tot} \approx 2.75\,M_\odot$. The HMNS could have persisted for the Alfvén crossing timescale of $\sim$1 s (Metzger et al. 2018), sufficiently long to power an sbGRB. Based on a suite of merger simulations targeted toward GW170817, Radice et al. (2018a) found that the remnant indeed most likely possessed enough angular momentum to prevent a collapse and to form a long-lived HMNS, even for $M_{\rm tot} \approx 2.75\,M_\odot$.

The region $M_{\rm tot} < 2.8\,M_\odot$ in Figure 2 summarizes this alternative scenario, in which sbGRBs arise from transient jets powered by moderately long-lived HMNSs formed from relatively low-mass binaries (left yellow region). In this scenario, all prompt-collapse BHs give rise to lbGRBs, where dimensional analysis suggests that M_d determines the jet power (Section 5.2).

4.3. Delayed-collapse BHs

In BNS mergers where the combined mass is $M_{\rm tot} \lesssim 2.8\,M_\odot$, the collapse of the HMNS into a BH may introduce a delayed launching of BZ jets, which could potentially contribute to the cbGRB populations. When the BH formation is preceded by a transient phase of an HMNS, the disk mass depends on $T_{\rm HMNS}$. If the HMNS collapses within a few milliseconds, the system evolves in a similar way to prompt-collapse BHs. A longer-lasting HMNS with $T_{\rm HMNS} \gtrsim 10$ ms allows for a greater opportunity for the postcollapse disk to grow through angular momentum transport to $M_d \approx 0.1\,M_\odot$ (e.g., Hotokezaka et al. 2013a). However, a longer-lived HMNS also provides an opportunity for the disk to lose mass prior to the BH formation. The disk continuously expands due to viscous angular momentum transport by the differentially rotating HMNS and viscous heating by magnetorotational instabilities (MRI) in the disk. Once neutrino cooling becomes subdominant to viscous heating, the disk expels winds, thereby reducing its mass (see, e.g., Siegel & Metzger 2018; Fernández et al. 2019b). In cases where vigorous viscous heating prompts rapid expansion, a substantial portion of the disk mass might be lost within $T_{\rm HMNS}$ (Fujibayashi et al. 2018, 2020).

The post-HMNS collapse disk mass remains elusive due to uncertainties pertaining to variables such as the magnetic field and effective viscosity in the disk, $T_{\rm HMNS}$, and other contributing factors. Given the significant impact of the disk mass on determining the cbGRB type, the role of delayed-collapse BHs remains uncertain.[16] Two possibilities exist. (i) If the disk mass is appreciably reduced by viscous heating prior to BH formation, then the BZ jet might be less luminous compared to the preceding HMNS-powered jet that generated the sbGRB. In such instances, the jets launched by delayed-collapse BHs could serve as sources of EE once they transition into the MAD state. (ii) If the viscous heating is insufficiently strong to remove the bulk of the disk mass on $T_{\rm HMNS}$ timescales, the BH forms with a massive disk. As outlined in Section 4.1, such disks are likely to give rise to lbGRBs. If this configuration characterizes the standard picture of HMNSs, the lbGRBs would supersede the observational imprint of HMNS-powered jets, indicating that all cbGRBs are powered by BHs. Interestingly, this perspective forecasts that BNS mergers with $M_{\rm tot} \lesssim 2.8\,M_\odot$ lead to lbGRBs, implying that lbGRBs are more common than sbGRBs.

[16] Notably, the disk mass ejection timescale may bear observable implications, as early mass ejection from the disk shortens the freeze-out time for the electron fraction. Therefore, in scenarios with intense viscous heating, the electron fraction equilibrium is lower (Fujibayashi et al. 2020), enabling us to estimate the disk mass at $T_{\rm HMNS}$ from kilonova observations.

4.4. Long-lived SMNSs

For particularly low-mass binaries, $M_{\rm tot} \lesssim 2.4\,M_\odot$, a very long-lived rigidly rotating SMNS with $M_d \approx 0.1\,M_\odot$ can form (Giacomazzo & Perna 2013; Foucart et al. 2016). Similar to the HMNS case, the early stages after the formation of an SMNS can, in principle, give rise to moderately relativistic outflows with $\Gamma \sim 10$ (e.g., Metzger et al. 2008b). However, SMNSs can live for $t \gg 1$ s before collapsing and thus may generate a relativistic wind that reaches $\Gamma \gtrsim 100$ as the rate of neutrino-driven mass ablation from the SMNS surface decays (e.g., Thompson et al. 2004; Metzger et al. 2008b). Relativistic MHD (Bucciantini et al. 2012) and numerical relativity (Ciolfi et al. 2017; Ciolfi 2020; Ruiz et al. 2020) simulations have demonstrated that long-lived magnetars are potentially capable of powering cbGRB jets. Such jets could be compatible with energy injection into cbGRB afterglows (Zhang & Mészáros 2001), and the late-time spin-down luminosity of the magnetar obeys $\sim t^{-2}$, also consistent with the observed decay evolution of the EE (Metzger et al. 2008b; Bucciantini et al. 2012; Gompertz et al. 2013).

The kilonovae that accompanied the two recent lbGRBs, GRB 211211A and GRB 230307A, support relatively slow outflows ($v_{\rm ej} \lesssim 0.1c$) containing high-opacity material consistent with significant lanthanide/actinide enrichment (Rastinejad et al. 2022; Levan et al. 2023a; Barnes & Metzger 2023). While both of these properties are consistent with the disk outflows from a BH accretion disk (e.g., Siegel & Metzger 2017; Fernández et al. 2019b), the ejecta velocities are too low compared to those expected following substantial energy injection from the magnetar wind (Bucciantini et al. 2012). Sustained neutrino irradiation of the disk outflows from the hot stable NS remnant also precludes significant heavy r-process material (e.g., Metzger & Fernández 2014; Kasen et al. 2015; Lippuner et al. 2017).

Additional arguments that disfavor SMNSs as the progenitors of the majority of the cbGRBs include (i) lack of evidence for a significant injection of rotational energy from the magnetar based on the late radio afterglow emission (Metzger & Bower 2014; Horesh et al. 2016; Schroeder et al. 2020; Beniamini & Lu 2021) and (ii) the BNS mass distribution favoring HMNSs as the common remnant of a BNS merger. Recent results by Margalit et al. (2022) show that accretion can shorten the SMNS lifetime such that it is closer to $T_{\rm HMNS}$, reducing the parameter space capable of generating long-lived magnetars. In light of the viability of the massive BH disk scenario, the above arguments disfavor the model suggested by Metzger et al. (2008b) and Sun et al. (2023), in which lbGRBs with EE are powered by long-lived magnetars.

4.5. Binary WD Merger and AIC

The formation of a magnetized NS does not require a merger that involves a preexisting NS. Instead, it may originate from the gravitational collapse of a WD in a binary system (Taam & van den Heuvel 1986). The secondary star for AIC can either be a merging WD companion or a nondegenerate donor (e.g., Duncan & Thompson 1992; Usov 1992; Yoon et al. 2007). The resulting newly formed NS can be a magnetar if the magnetic field of the progenitor WD is very strong and amplified by flux

freezing during (see, e.g., Burrows et al. 2007) or after the collapse through magnetic winding or other dynamo action after the merger/collapse. Magnetars formed from AIC may potentially act as central engines for cbGRBs (Usov 1992; Metzger et al. 2008b).

Accreting WDs are generally considered to lose much of their angular momentum during their evolution (e.g., through classical nova eruptions), ultimately becoming slow rotators (Berger et al. 2005). In the case of binary WD mergers, the angular momentum budget is initially much higher; however, the most massive mergers capable of undergoing AIC ultimately produce an NS with a mild rotation period of $\sim$10 ms, due to angular momentum redistribution during the postmerger phase prior to collapse (Schwab 2021). Such slowly rotating magnetars have a limited energy reservoir and would not be accompanied by an appreciable accretion disk.

AIC occurs when a massive oxygen–neon WD accretes matter from a companion star until it reaches the Chandrasekhar limit and collapses into an NS (e.g., Nomoto & Kondo 1991; however, see Jones et al. 2016). During the collapse process, conservation of angular momentum may lead to the formation of a rapidly spinning NS surrounded by a disk (Bailyn & Grindlay 1990). Additionally, the fast and differential rotation in the newly formed NS results in a substantial amplification of the magnetic field (Dessart et al. 2007), which may result in a millisecond magnetar. However, the AIC faces similar challenges as the SMNS scenario (Section 4.4). For example, neutrino irradiation from the long-lived magnetar will increase the electron fraction in the disk outflows (e.g., Metzger et al. 2009; Darbha et al. 2010), leading to inconsistencies with the lanthanide-rich ejecta inferred from the kilonova emission from GRB 211211A to GRB 230307A.

Another scenario involving WDs is an NS–WD merger (Fryer et al. 1999; King et al. 2007), which was proposed as the origin of GRB 211211A (Yang et al. 2022) and possibly GRB 230307A (Sun et al. 2023). It is argued that the burst duration scales with the accretion timescale, which in turn scales inversely with the density of the companion star for an accretion-powered engine, favoring a WD. However, as we have shown in Section 3, the burst timescale depends on the disk mass and the magnetic flux threading the BH and does not necessarily require a low-density WD to prolong the accretion timescale. In fact, we find that after $t \sim 100$ ms, the mass accretion rate follows a single power-law profile, indicating that there is no accretion timescale relevant to cbGRBs. Additionally, proton-rich matter accreted from the disrupted WD is unlikely to reach high enough densities to produce neutron-rich outflows capable of generating any significant r-process material, much less the relatively heavy lanthanides (Metzger 2012; see Fernández et al. 2019a for simulations of the postmerger disk evolution and nucleosynthesis). The NS–WD merger scenario thus faces difficulties in explaining the observed kilonova emission (see Barnes & Metzger 2023, and references therein).

4.6. Neutrino Annihilation

The high accretion rates anticipated in postmerger disks give rise to strong neutrino emission. Efficient annihilation of neutrinos and antineutrinos can generate relativistic jets that may power cbGRBs (e.g., Woosley 1993). These jets are expected to operate as long as the accretion rate is $\dot{M} \gtrsim 10^{-2}\ M_{\odot}$ (Popham et al. 1999). This requirement implies that massive disks are necessary (e.g., Leng & Giannios 2014) to enable jet launching for $T_{90} \lesssim 1$ s. If the initial magnetic field in the disk is predominantly toroidal, the BZ jet may follow the neutrino-driven jet after $t \gtrsim 1$ s (e.g., Christie et al. 2019; Gottlieb et al. 2023a) and power the late EE (Barkov & Pozanenko 2011). This scenario cannot explain lbGRBs and, as we now argue, is also disfavored as the origin of sbGRBs.

The main limitation of neutrino-driven jets lies in their available energy (Leng & Giannios 2014; Just et al. 2016). In BNS mergers, where a significant amount of ejecta is expected along the polar axis, these low-energy jets would fail to break out and generate a cbGRB (Just et al. 2016). Furthermore, the mass distribution of the Galactic BNS population suggests that most postmerger remnants are HMNSs. The large amount of mass in the HMNS atmosphere (Section 4.2) would load neutrino-driven jets with baryons, hindering their ability to achieve relativistic velocities (Dessart et al. 2009). Consequently, such jets would be incapable of producing cbGRBs.

5. Origin of the Precursor Flare and Extended Emission and Comparison of BH- and HMNS-powered Jets

Figure 3 utilizes the light curves of lbGRB 211211A (black) and sbGRB 160821B (gray) to illustrate the connection between the underlying physics of the compact object (orange labels) and the various phases observed in the cbGRB light curve (yellow for sbGRBs, blue for lbGRBs, and green for preceding and succeeding phases). An sbGRB can be powered either by a BH with a light accretion disk or—as inferred by the kilonova observations of GRB 160821B—by a long-lived HMNS (Lamb et al. 2019), before collapsing into a BH. An lbGRB is fueled by a BH surrounded by a massive accretion disk, as the dimensionless magnetic flux threading the BH steadily accumulates. The origin of the precursor flare and the EE are discussed below.

Up to this point, we have presented both HMNS- and BH-powered jets as potential contributors to sbGRBs. However, there is no evidence indicating the existence of two distinct subpopulations among sbGRBs, suggesting that only one of these engines is responsible for producing the majority of sbGRBs. Table 1 summarizes the origin of sbGRBs and lbGRBs, as well as the outcomes of the different types of mergers, as predicted in both scenarios. We denote the scenario in which HMNSs power sbGRBs and BHs power lbGRBs as the "hybrid" scenario. The scenario in which all cbGRBs are powered by BHs, with the GRB duration increasing with the disk mass, is denoted as the "all-BH" scenario. Both scenarios predict the formation of an lbGRB when the BH is surrounded by a massive disk. When a less massive disk is present (in nearly equal mass ratio BNS mergers with $M_{\rm tot} \gtrsim 2.8\,M_{\odot}$ or BH–NS mergers with either high q or low a), the all-BH scenario predicts an sbGRB signal, whereas the hybrid scenario predicts an lbGRB signal. When $M_{\rm tot} \lesssim 2.8\,M_{\odot}$, the cbGRB duration in the all-BH scenario depends on the uncertain post-HMNS collapse disk mass (see Section 4.3).

In the all-BH scenario, the cbGRB duration spans a continuous spectrum, whereas in the hybrid scenario, the BH-powered lbGRBs comprise a separate class. Therefore, the hybrid scenario offers a natural distinction between sbGRBs powered by HMNSs and lbGRBs powered by BHs. Furthermore, the hybrid scenario finds support from the

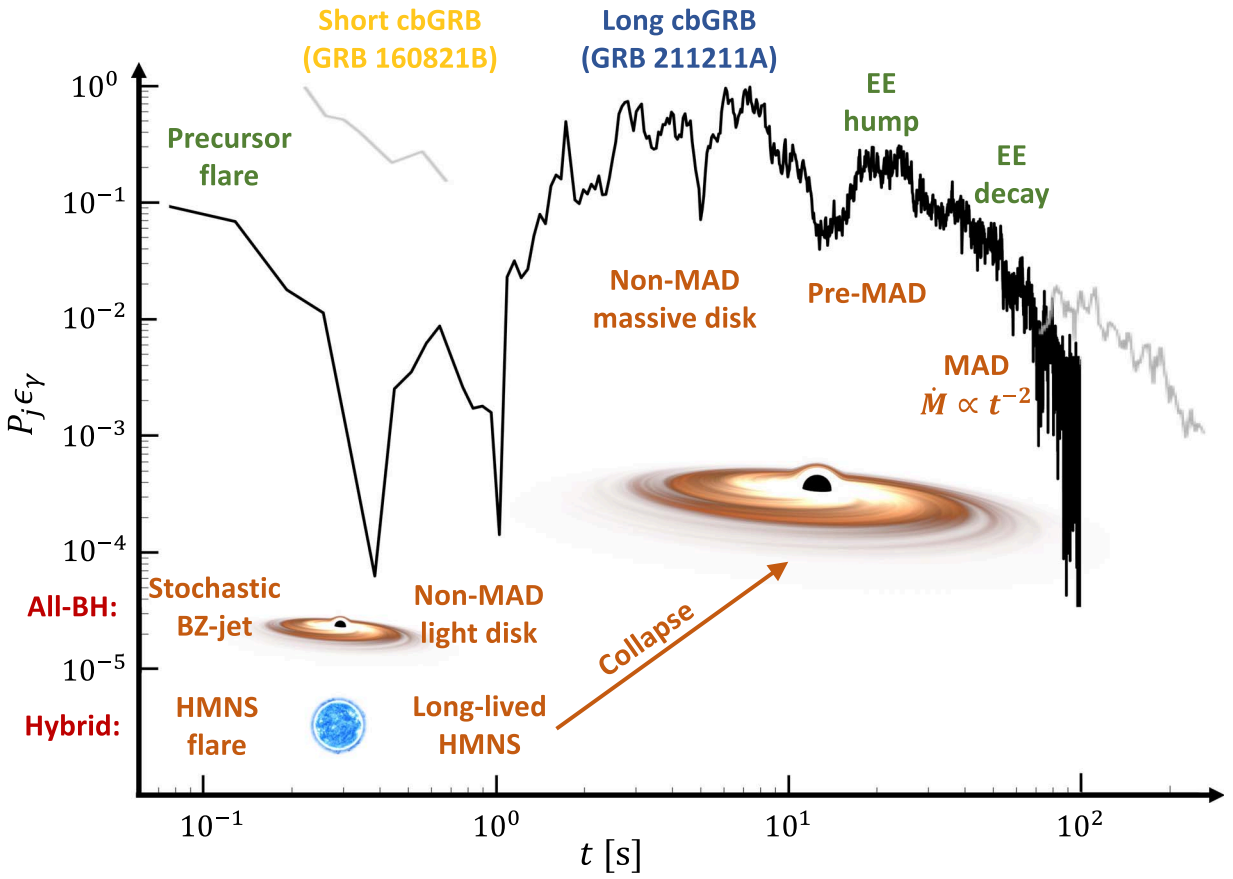

Figure 3. An illustration of how the underlying physics of the merger product (orange) in the hybrid and all-BH scenarios (red) translates into different phases in the cbGRB light curves: sbGRBs (yellow), lbGRBs (blue), and preceding and succeeding phases (green). The precursor flare (Section 5.1) can be generated either by the accumulation of a stochastic magnetic field on a BH (Gottlieb et al. 2023a) or by an HMNS (Most & Quataert 2023). An sbGRB can be powered either by a BH surrounded by a nonmassive disk before it transitions to a MAD state (Section 4.1) or by a long-lived HMNS (Section 4.2). On the other hand, an lbGRB emerges from BHs with massive disks before they enter the MAD state (Section 2), whether the BH formed promptly in the all-BH scenario or followed an HMNS collapse in the hybrid scenario. Finally, the BH disk becomes MAD and follows $P_j \sim t^{-2}$ to power the EE. Representations of the light curves of the lbGRB 211211A (Rastinejad et al. 2022) and sbGRB 160821B (Stanbro & Meegan 2016) are shown in black and gray, respectively, in a log-log scale. Both are confirmed to be cbGRBs by their detected kilonova counterparts (Lamb et al. 2019; Rastinejad et al. 2022).

Table 1
Summary of the Mapping between the Hybrid and All-BH Scenarios and Associated cbGRB Classes

Event Type		Scenario	
		Hybrid	All-BH
sbGRB engine		HMNS	BH + $M_d \lesssim 10^{-2}\,M_\odot$
lbGRB engine		BH + $M_d \approx 10^{-1}\,M_\odot$	
BNS	$M_{\rm tot} \lesssim 2.8\,M_\odot$; $q \lesssim 1.2$	sbGRB	sbGRB
	$M_{\rm tot} \lesssim 2.8\,M_\odot$; $q \gtrsim 1.2$	sbGRB	lbGRB
	$M_{\rm tot} \gtrsim 2.8\,M_\odot$; $q \lesssim 1.2$	lbGRB	sbGRB
	$M_{\rm tot} \gtrsim 2.8\,M_\odot$; $q \gtrsim 1.2$	lbGRB	lbGRB
BH–NS	Low q and high a	lbGRB	lbGRB
	High q $\oplus$ low a	lbGRB	sbGRB
	High q and low a	No GRB	No GRB

Note.
$\oplus$ denotes either or (XOR).

bimodal cbGRB duration distribution, the mass distribution of BNS systems, and observations and simulations of GW170817. In the following subsections, we show that the hybrid scenario is also more compatible than the all-BH scenario with all phases of the cbGRB light curve.

5.1. Precursor Flare

Each of the proposed hybrid and all-BH scenarios postulates a different physical origin for the precursor flare before the rise of the main burst. In the hybrid scenario, Most & Quataert (2023) demonstrated how the differentially rotating HMNS builds loops with footpoints at different latitudes on its surface. The resultant twist in the loop causes it to become unstable, inflate, and buoyantly rise, forming a bubble that is entirely detached from the HMNS surface and erupts after reconnecting (e.g., Carrasco et al. 2019; Mahlmann et al. 2023; Most & Quataert 2023). This behavior powers quasiperiodic flares prior to the jet formation.

For BH-powered jets, Gottlieb et al. (2023a) showed that if the seed magnetic field in the disk is toroidal, as expected in binary systems, then the stochastic accumulation of incoherent magnetic loops on the horizon can lead to a short burst of energy (see model T_s in their Figure 1(d)), which may constitute the precursor flare. As more flux reaches the BH, the stochastic field cancels out by virtue of the contribution of loops of different polarity. Consequently, the total flux drops to zero before starting to build a large-scale poloidal field through the dynamo process and power the cbGRB emission. Due to the stochastic nature of the accumulated flux, the flare energy is expected to be very weak, and the resultant outflow may not be

able to punch through the optically thick disk wind and/or dynamical ejecta (Gottlieb et al. 2023a). Therefore, the emergence of such precursor flares in the all-BH scenario may require fine-tuning. Nevertheless, it is possible that the precursor in the all-BH scenario is also powered by a short-lived HMNS before it collapses into a BH on an $\sim$10 ms timescale.

5.2. Main cbGRB Burst

Dimensional analysis suggests that $\Phi \sim \sqrt{M_d}$, thus $M_d \sim \Phi^2 \sim P_j^2$, while the dimensionless magnetic flux ϕ is independent of M_d. This is also supported by the fact that the saturation level of the amplified ordered field in the disk seems to scale with the turbulent disk pressure, which in turn likely scales with $\dot{M}$. This implies that reducing the disk mass results in a lower jet power, rather than shortening the cbGRB duration, which scales with the dimensionless magnetic flux (see Section 3). Namely, massive disks produce GRB 211211A-like lbGRBs, whereas lower-mass disks produce less luminous lbGRBs, which are harder to detect. Therefore, unless there is an intrinsic correlation between M_d and ϕ, the variation in M_d does not naturally yield the variation in the cbGRB duration. This favors BHs with less massive disks to power weaker lbGRBs and sbGRBs as a distinct cbGRB population that emerges from HMNSs.

5.3. Extended Emission

Following the main hard burst, the softer EE phase commences. In both hybrid and all-BH scenarios, an accretion disk forms and is present at the time of the EE. Once the disk enters the MAD state, the jet power evolves in accordance with the mass accretion rate, $P_j \sim t^{-2}$, similar to the observed temporal evolution of the EE decay. The preceding flat EE hump is thus generated by the constant power jet, just before the disk transitions to a MAD state. The EE may end once the disk is overheated after $\sim$100 s and evaporates on this timescale (Lu & Quataert 2023). This evolution of a constant jet power followed by a t^{-2} decay for another order of magnitude in time naturally results in a comparable energy content between the cbGRB prompt emission and the EE, as suggested by observations (Kaneko et al. 2015).

Any cbGRB model must account for the reason why the EE likely emerges $\sim$10 s after the onset of the prompt emission. This implies that if the EE follows an sbGRB where $T_{90} \ll 10$ s, there must be a quiescent period between the prompt and the EE phases (e.g., Perley et al. 2009). The all-BH scenario, which posits that both cbGRB types are powered by BHs, encounters difficulties in explaining this constraint. As described in Section 3, BHs launch jets with a constant power followed immediately by the EE decay once the disk transitions to a MAD state. Therefore, no quiescent times would be expected to emerge between the prompt emission and the EE phase. In the hybrid model, sbGRBs are powered by HMNSs, and the postcollapse BZ jet generates the EE. The time between the HMNS collapse and the launch of the BZ jet offers a natural explanation for the occurrence of the observed quiescent interval.

6. Conclusions

The discoveries of $\sim$10 s long prompt emission in lbGRBs 211211A (Rastinejad et al. 2022) and 230307A (Levan et al. 2023a), followed by softer EE signals, suggest that the cbGRB population can be divided into two classes: sbGRBs ($T_{90} \lesssim 1$ s) and lbGRBs ($T_{50} \sim 10$ s). However, the underlying physics that differentiates these classes and the origin of the prolonged EE are poorly understood. Moreover, drawing inferences about the astrophysical properties of binary mergers from cbGRB observables poses a formidable challenge. In this paper, we have developed a novel theoretical framework that connects different binary merger types to the distinct subpopulations of cbGRBs and the different components in their light curves. This provides the very first solution for the origin of both the constant power prompt emission and decaying EE from first principles.

In collapsars, the presence of a dense stellar core surrounding the BH hinders the launching of jets when the accretion disk is not in a MAD state. This implies that for lGRBs, the jet operates in a MAD state at all times, and the characteristic lGRB duration can be set by either the mass accretion rate or the BH spin-down timescale. By contrast, in binary systems, where the environment is less dense, the conditions allow for the launching of the jet before the disk enters the MAD state. Due to the compactness of the disk, the dimensional magnetic flux, Φ, quickly accumulates on the BH, resulting in a roughly constant jet power before the transition to MAD occurs. After the accretion disk enters the MAD state, the jet power follows the mass accretion rate of $P_j \sim \dot{M} \sim t^{-2}$, signaling the end of the prompt emission phase and the onset of the decaying EE. This behavior is consistently observed in all first-principles simulations and should be considered when modeling cbGRB jets. In this jet power evolution model, there are two free parameters: (i) the time of the transition to a MAD state, which determines the cbGRB duration and is influenced by ϕ, and (ii) the magnitude of the constant jet power, which is governed by Φ.

The nature of the resultant central engine is determined by the total mass of the binary system. Unequal mass ratio BNS mergers with $M_{\rm tot} \gtrsim 2.8\,M_\odot$ and BH–NS mergers with a moderate mass ratio and high premerger BH spin lead to the formation of a BH surrounded by a massive ($M_d \gtrsim 0.1\,M_\odot$) accretion disk. Depending on Φ (as illustrated in Figure 1), such a massive disk can give rise to either extremely bright sbGRBs or lbGRBs. Analyzing the sbGRB and lbGRB observational data, we conclude that massive disks inevitably power long-duration signals and thus are most likely the progenitors of lbGRBs such as GRB 211211A and GRB 230307A. Lighter disks with $M_d \lesssim 10^{-2}\,M_\odot$ can produce typical sbGRBs.

In other merger configurations, the resultant BH disk is less massive, and if Φ is weakly dependent on M_d, an sbGRB jet can be generated. While this interpretation of cbGRBs powered by BHs provides an explanation for sbGRBs and lbGRBs, it faces challenges in explaining various observational features in cbGRB light curves, including flares observed before the prompt emission and the quiescent time observed between the prompt emission and the EE. Most importantly, the Galactic BNS population suggests that most binary systems have $M_{\rm tot} \lesssim 2.75\,M_\odot$ (e.g., Özel et al. 2012; Kiziltan et al. 2013), where a prompt collapse into a BH is not anticipated.

In BNS mergers with $M_{\rm tot} \lesssim 2.8\,M_\odot$, the product of the merger is an HMNS (e.g., Margalit & Metzger 2019). Both analytic and numerical studies demonstrated that HMNSs are capable of generating relativistic jets that power cbGRBs (e.g.,

Metzger et al. 2008b; Kiuchi et al. 2023). The best-studied event in this mass range is the multimessenger GW170817 with $M_{\rm tot} \approx 2.75\,M_\odot$. The associated kilonova signal observed in GW170817 supports the formation of a long-lived ($T_{\rm HMNS} \lesssim 1$ s) HMNS (Radice et al. 2018b; Metzger et al. 2018). This timescale is sufficiently long to power sbGRBs. Unlike BHs, HMNSs can naturally produce precursor flares (Most & Quataert 2023) and account for the quiescent time between the prompt and the EE by virtue of the transition from HMNS- to BH-powered jets.

Various constraints, from kilonova observations to radio constraints on late-time rotational energy injection, favor prompt-collapse BH- and HMNS-powered jets over models that include long-lived magnetars, WDs, or neutrino-driven jets. While we thus find it likely that BHs with massive disks are responsible for lbGRBs, we are less certain about the origin of the shorter sbGRB population. A priori, both BH-powered jets (BH–NS mergers or BNS mergers with $M_{\rm tot} \gtrsim 2.8\,M_\odot$ and $q \lesssim 1.2$) and HMNS-powered jets ($M_{\rm tot} \lesssim 2.8\,M_\odot$) remain viable possibilities (Figure 2 and Table 1). However, the lack of evidence for two distinct subclasses among the sbGRB population suggests that if HMNS-powered jets are different than BH-powered jets, then one of these channels dominates. We find several reasons to prefer transient HMNSs over low disk mass BHs in this case.

A key distinction between the all-BH and hybrid scenarios lies in the cbGRB duration distribution. BH-powered jets should exhibit a continuous spectrum from sbGRBs to lbGRBs, scaling with the binary mass ratio. Conversely, if HMNSs are the progenitors of sbGRBs, they differ intrinsically from BH-powered lbGRBs, proposing two distinct cbGRB classes. The recent joint detections of cbGRBs with kilonovae provide an exciting opportunity to assemble a sizable sample of confirmed cbGRB events. Analyzing this collection could shed light on whether kilonova-associated sbGRBs and lbGRBs form a continuous spectrum or represent distinct classes. This, in turn, may enable us to deduce whether HMNSs, BHs, or both serve as the primary progenitors of sbGRBs.

Acknowledgments

We thank the referee, Alexander Tchekhovskoy, Rosalba Perna, Jonatan Jacquemin-Ide, Om Sharan Salafia, and Daniel Kasen for valuable discussions. We thank Jillian Rastinejad for providing the observational data for GRB 211211A. O.G. is supported by Flatiron Research and CIERA Fellowships. O.G. acknowledges support by Fermi Cycle 14 Guest Investigator program 80NSSC22K0031 and NSF grant AST-2107839. B.D. M. acknowledges support from the National Science Foundation (grant No. AST-2002577). D.I. is supported by Future Investigators in NASA Earth and Space Science and Technology (FINESST) award No. 80NSSC21K1851. An award of computer time was provided by the ASCR Leadership Computing Challenge (ALCC), Innovative and Novel Computational Impact on Theory and Experiment (INCITE), and OLCF Director's Discretionary Allocation programs under award PHY129. This research used resources of the National Energy Research Scientific Computing Center, a DOE Office of Science User Facility supported by the Office of Science of the U.S. Department of Energy under contract No. DE-AC02-05CH11231 using NERSC awards ALCC-ERCAP0022634 and NP-ERCAP0020543 (allocation m2401). This research was facilitated by the Multimessenger Plasma Physics Center (MPPC), NSF grant PHY-2206610.

Appendix
Binary Merger Simulations

Our simulation setup is similar to that described in Gottlieb et al. (2023a, 2023b). Below, we summarize the setup and main properties of the simulations. We employ a numerical relativity simulation performed with the SpEC code (SpEC collaboration 2023) that evolves the system from the premerger phase to 10 ms after the prompt collapse to a BH. In the BNS merger simulations, the masses of the merging NSs are 1.06 and $1.78\,M_\odot$, and the NSs are described with the LS220 EoS (Lattimer & Swesty 1991). The merger product is a BH with mass $M_{\rm BH} = 2.67\,M_\odot$ and dimensionless spin $a = 0.68$. The BH is surrounded by a massive accretion disk of $M_d = 0.096\,M_\odot$. Details of the SpEC simulation can be found in Foucart et al. (2023). The merger simulation includes general relativity (GR), relativistic fluid dynamics, Monte Carlo neutrino transport, and a subgrid viscosity model to approximate angular momentum transport and heating due to MHD instabilities. In the BH–NS merger simulation, the mass of the NS is $1.35\,M_\odot$, and the mass of the BH is $4.05\,M_\odot$. The BH begins with a dimensionless premerger spin of $a = 0.087$. Here, we describe the NS using an SFHo EoS (Steiner et al. 2013). The simulation evolves for just under 5.75 orbits before the system reaches merger. Upon evolving the system to 10 ms postmerger, the BH exhibits a mass of $M_{\rm BH} = 5.26\,M_\odot$ and a spin of $a = 0.59$. The disrupted NS results in a disk mass of $M_d = 0.007\,M_\odot$.

At 10 ms after the collapse, we follow the scheme described in Gottlieb et al. (2023a) to remap the numerical relativity output to the GPU-accelerated GR-MHD code H-AMR (Liska et al. 2022), where we simulate the postmerger evolution for an additional $\sim$1 s. At the time of remapping, we introduce magnetic fields into the accretion disk. We explore various field configurations, where the geometry can be either toroidal or poloidal, and the field profile depends on the radius and mass density with a cutoff at 5×10^{-4} of the maximum density at the time of remapping. We verify that the fastest-growing MRI mode's wavelength is resolved in all simulations at all times. Table 2 summarizes the considered configurations.

Table 2
A Summary of the Models' Parameters

Model	Merger	q	$M_{\rm tot}$	A	β_p	t_f (s)
NN $-$ P_w	BNS	1.7	2.84	$A_\varphi \propto \rho^2 r^3$	$10^{3.5}$	1.3
NN $-$ P_c	BNS	1.7	2.84	$A_\varphi \propto \rho^2 r^6$	$10^{2.5}$	1.2
NN $-$ P_s	BNS	1.7	2.84	$A_\varphi \propto \rho^2 r^3$	$10^{1.5}$	0.8
NN $-$ T_c	BNS	1.7	2.84	$A_\theta \propto \rho r^2$	10	1.3
NN $-$ T_s	BNS	1.7	2.84	$A_\theta \propto \rho r^2$	1	1.2
BN $-$ P_w	BH–NS	3.0	5.4	$A_\varphi \propto \rho r^2$	10^5	1.0
BN $-$ P_c	BH–NS	3.0	5.4	$A_\varphi \propto \rho r^2$	10^3	0.7
BN $-$ P_s	BH–NS	3.0	5.4	$A_\varphi \propto \rho r^2$	10^2	1.0
BN $-$ T_c	BH–NS	3.0	5.4	$A_\theta \propto \rho r^2$	10^2	1.2
BN $-$ T_s	BH–NS	3.0	5.4	$A_\theta \propto \rho r^2$	1	1.1

Note. The model names stand for merger type BNS (NN) or BH–NS (BN) and poloidal (P) or toroidal (T) initial magnetic field, with the subscripts indicating the strength of the field: weak (w), canonical (c), or strong (s). q is the mass ratio, $M_{\rm tot}$ is the total binary mass, A is the vector potential, β_p is the characteristic gas-to-magnetic pressure ratio, and t_f is the final time of the simulation with respect to the merger time.

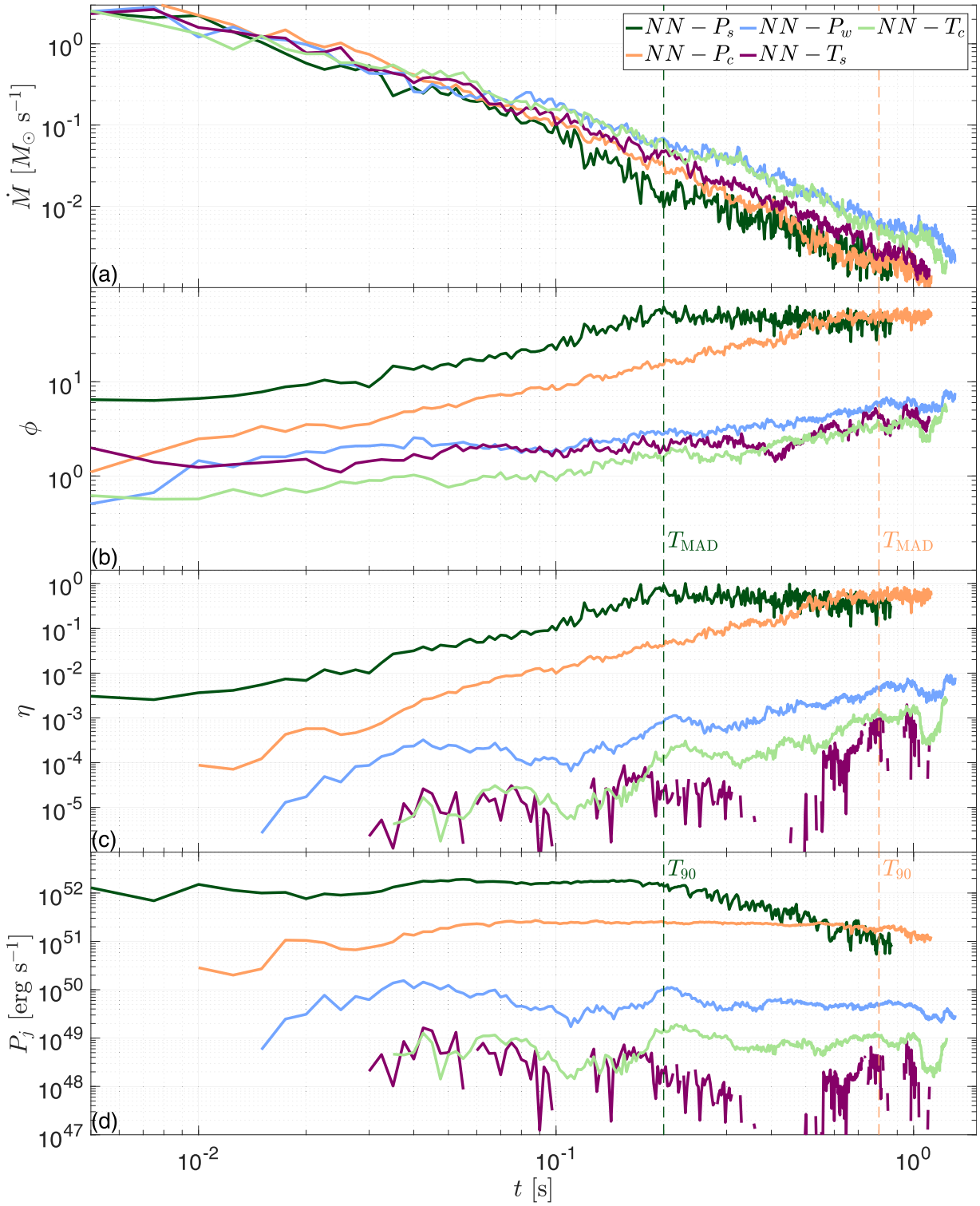

Figure 4. Time evolution on the BH horizon for different models. Panel (a): The mass accretion rate in all models follows $\dot{M} \approx (t/0.01\ \mathrm{s})^{-2}$. Panel (b): The dimensionless magnetic flux $\phi = \Phi/\sqrt{\dot{M}cr_g^2}$ shows a gradual increase until entering the MAD state at $\phi \approx 50$ (vertical dashed lines), after which it remains roughly constant. Panel (c): The jet launching efficiency $\eta \equiv \eta_\phi \eta_a$ increases gradually with ϕ until it reaches the maximum launching efficiency $\eta \approx 0.4$ in the MAD state. Panel (d): The jet power, $P_j = \eta \dot{M} c^2$, is roughly constant due to constant dimensional magnetic flux threading the BH. Once the disk becomes MAD, η saturates, and the jet power drops as $P_j \sim \dot{M} \sim t^{-2}$ (vertical dashed lines).

The H-AMR grid in spherical-polar coordinates is uniform in $\log r$, θ, and φ, extending from $r = r_g$ to $10^5 r_g$. The base grid resolution is $N_r \times N_\theta \times N_\varphi = 384 \times 96 \times 96$ cells. Using static mesh refinement, we double the base resolution (quadruple in model T_c) in all dimensions at $4 < r/r_g < 100$. By using three levels of adaptive mesh refinement, we properly resolve the relativistic outflows.

Figures 4 and 5 depict the temporal evolution of various properties on the BH horizon in the BNS and BH–NS merger simulations, respectively. Panels (a) display the mass accretion

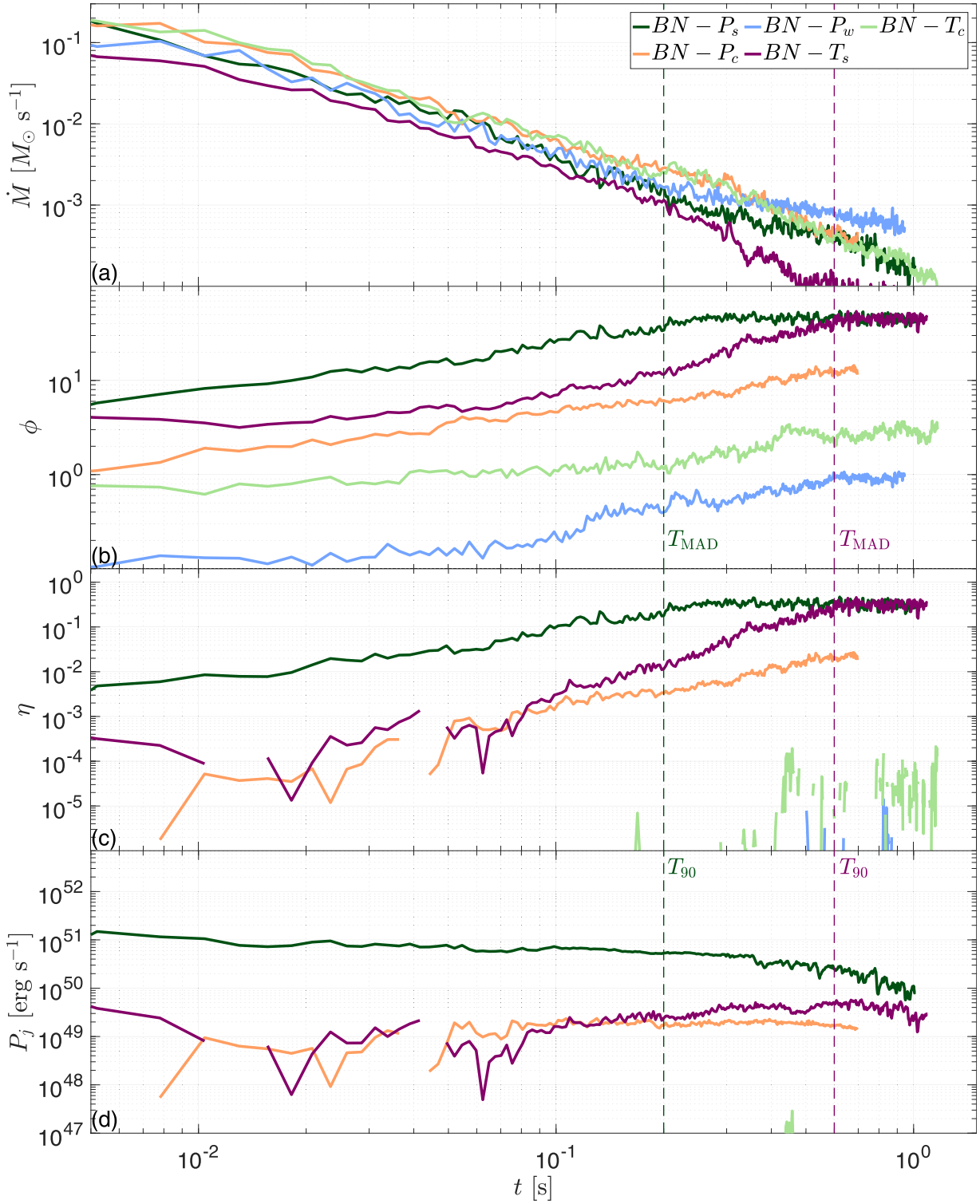

Figure 5. Same as Figure 4 but for the BH–NS merger simulations.

rate, featuring a power-law decay of $\dot{M} \sim t^{-2}$. Panels (b) illustrate that the constant dimensional flux threading the BH leads to a gradual growth of the dimensionless flux ϕ with the decline in $\dot{M}$. Consequently, the jet launching efficiency, $\eta = \eta_a \eta_\phi$, steadily increases, as shown in panels (c). Once the flux reaches saturation at $\phi \approx 50$ (vertical dashed lines), or $\eta = \eta_a \approx 0.3\,(0.4)$ for $a = 0.59\,(0.68)$, the disk enters a MAD state, and the BH achieves its maximum jet launching efficiency. As indicated in panels (d), the jet power remains roughly constant at all times before the disk turns MAD, owing to a constant Φ on the BH (Equation (1)). As demonstrated by the strong poloidal field models, P_s and P_c, the saturation of ϕ (or drop in Φ) at $t > T_{\rm MAD}$ leads to $P_j \sim t^{-2}$ (Equation (2)). Eventually, all models will reach a MAD state within several seconds, marking the typical prompt duration. Models with initial toroidal magnetic configuration in the disk exhibit stronger variability in the light curve, offering a possible origin of the variability observed in cbGRB light curves.

ORCID iDs

Ore Gottlieb https://orcid.org/0000-0003-3115-2456
Brian D. Metzger https://orcid.org/0000-0002-4670-7509
Eliot Quataert https://orcid.org/0000-0001-9185-5044
Danat Issa https://orcid.org/0009-0005-2478-7631
Tia Martineau https://orcid.org/0000-0002-1025-8318
Francois Foucart https://orcid.org/0000-0003-4617-4738
Matthew D. Duez https://orcid.org/0000-0002-0050-1783
Lawrence E. Kidder https://orcid.org/0000-0001-5392-7342
Harald P. Pfeiffer https://orcid.org/0000-0001-9288-519X
Mark A. Scheel https://orcid.org/0000-0001-6656-9134

References

Abbott, B. P., Abbott, R., Abbott, T. D., et al. 2019, PhRvX, 9, 011001
Abbott, B. P., Abbott, R., Abbott, T. D., et al. 2020, LRR, 23, 3
Abbott, R., Abbott, T. D., Abraham, S., et al. 2021, ApJL, 913, L7
Ackermann, M., Asano, K., Atwood, W. B., et al. 2010, ApJ, 716, 1178
Aguilera-Miret, R., Palenzuela, C., Carrasco, F., & Viganò, D. 2023, PhRvD, 108, 103001
Ahumada, T., Singer, L. P., Anand, S., et al. 2021, NatAs, 5, 917
Bailyn, C. D., & Grindlay, J. E. 1990, ApJ, 353, 159
Barkov, M. V., & Pozanenko, A. S. 2011, MNRAS, 417, 2161
Barnes, J., & Metzger, B. D. 2023, ApJ, 947, 55
Bauswein, A., Baumgarte, T. W., & Janka, H. T. 2013, PhRvL, 111, 131101
Belczynski, K., Taam, R. E., Rantsiou, E., & van der Sluys, M. 2008, ApJ, 682, 474
Beniamini, P., & Lu, W. 2021, ApJ, 920, 109
Beniamini, P., Nava, L., Duran, R. B., & Piran, T. 2015, MNRAS, 454, 1073
Beniamini, P., Nava, L., & Piran, T. 2016, MNRAS, 461, 51
Berger, E. 2014, ARA&A, 52, 43
Berger, L., Koester, D., Napiwotzki, R., Reid, I. N., & Zuckerman, B. 2005, A&A, 444, 565
Biscoveanu, S., Burns, E., Landry, P., & Vitale, S. 2023, RNAAS, 7, 136
Blandford, R. D., & Znajek, R. L. 1977, MNRAS, 179, 433
Bromberg, O., Nakar, E., & Piran, T. 2011, ApJL, 739, L55
Bromberg, O., Nakar, E., Piran, T., & Sari, R. 2012, ApJ, 749, 110
Bromberg, O., Nakar, E., Piran, T., & Sari, R. 2013, ApJ, 764, 179
Bucciantini, N., Metzger, B. D., Thompson, T. A., & Quataert, E. 2012, MNRAS, 419, 1537
Burrows, A., Dessart, L., Livne, E., Ott, C. D., & Murphy, J. 2007, ApJ, 664, 416
Carrasco, F., Viganò, D., Palenzuela, C., & Pons, J. A. 2019, MNRAS, 484, L124
Christie, I. M., Lalakos, A., Tchekhovskoy, A., et al. 2019, MNRAS, 490, 4811
Ciolfi, R. 2020, MNRAS, 495, L66
Ciolfi, R., Kastaun, W., Giacomazzo, B., et al. 2017, PhRvD, 95, 063016
Ciolfi, R., Kastaun, W., Kalinani, J. V., & Giacomazzo, B. 2019, PhRvD, 100, 023005
Combi, L., & Siegel, D. M. 2023, arXiv:2303.12284
Darbha, S., Metzger, B. D., Quataert, E., et al. 2010, MNRAS, 409, 846
Della Valle, M., Chincarini, G., Panagia, N., et al. 2006, Natur, 444, 1050
Dessart, L., Burrows, A., Livne, E., & Ott, C. D. 2007, ApJ, 669, 585
Dessart, L., Ott, C. D., Burrows, A., Rosswog, S., & Livne, E. 2009, ApJ, 690, 1681
Dietrich, T., Bernuzzi, S., Ujevic, M., & Brügmann, B. 2015, PhRvD, 91, 124041
Dietrich, T., Ujevic, M., Tichy, W., Bernuzzi, S., & Brügmann, B. 2017, PhRvD, 95, 024029
Duez, M. D., Foucart, F., Kidder, L. E., Ott, C. D., & Teukolsky, S. A. 2010, CQGra, 27, 114106
Duncan, R. C., & Thompson, C. 1992, ApJL, 392, L9
Eichler, D., Livio, M., Piran, T., & Schramm, D. N. 1989, Natur, 340, 126
Etienne, Z. B., Faber, J. A., Liu, Y. T., et al. 2008, PhRvD, 77, 084002
Etienne, Z. B., Paschalidis, V., & Shapiro, S. L. 2012, PhRvD, 86, 084026
Farrow, N., Zhu, X.-J., & Thrane, E. 2019, ApJ, 876, 18
Fernández, R., Foucart, F., Kasen, D., et al. 2017, CQGra, 34, 154001
Fernández, R., Foucart, F., & Lippuner, J. 2020, MNRAS, 497, 3221
Fernández, R., Margalit, B., & Metzger, B. D. 2019a, MNRAS, 488, 259
Fernández, R., Quataert, E., Schwab, J., Kasen, D., & Rosswog, S. 2015, MNRAS, 449, 390
Fernández, R., Tchekhovskoy, A., Quataert, E., Foucart, F., & Kasen, D. 2019b, MNRAS, 482, 3373
Fong, W., Berger, E., Margutti, R., & Zauderer, B. A. 2015, ApJ, 815, 102
Foucart, F. 2012, PhRvD, 86, 124007
Foucart, F., Deaton, M. B., Duez, M. D., et al. 2013, PhRvD, 87, 084006
Foucart, F., Deaton, M. B., Duez, M. D., et al. 2014, PhRvD, 90, 024026
Foucart, F., Desai, D., Brege, W., et al. 2017, CQGra, 34, 044002
Foucart, F., Duez, M. D., Haas, R., et al. 2023, PhRvD, 107, 103055
Foucart, F., Duez, M. D., Kidder, L. E., et al. 2012, PhRvD, 85, 044015
Foucart, F., Duez, M. D., Kidder, L. E., et al. 2019, PhRvD, 99, 103025
Foucart, F., Duez, M. D., Kidder, L. E., & Teukolsky, S. A. 2011, PhRvD, 83, 024005
Foucart, F., Haas, R., Duez, M. D., et al. 2016, PhRvD, 93, 044019
Foucart, F., Hinderer, T., & Nissanke, S. 2018, PhRvD, 98, 081501
Fragione, G. 2021, ApJL, 923, L2
Fryer, C. L., Woosley, S. E., Herant, M., & Davies, M. B. 1999, ApJ, 520, 650
Fujibayashi, S., Kiuchi, K., Nishimura, N., Sekiguchi, Y., & Shibata, M. 2018, ApJ, 860, 64
Fujibayashi, S., Wanajo, S., Kiuchi, K., et al. 2020, ApJ, 901, 122
Galama, T. J., Vreeswijk, P. M., van Paradijs, J., et al. 1998, Natur, 395, 670
Gal-Yam, A., Fox, D. B., Price, P. A., et al. 2006, Natur, 444, 1053
Gao, H., Lei, W.-H., & Zhu, Z.-P. 2022, ApJL, 934, L12
Giacomazzo, B., & Perna, R. 2013, ApJL, 771, L26
Giblin, T. W., Connaughton, V., van Paradijs, J., et al. 2002, ApJ, 570, 573
Goldreich, P., & Julian, W. H. 1969, ApJ, 157, 869
Gompertz, B. P., O'Brien, P. T., Wynn, G. A., & Rowlinson, A. 2013, MNRAS, 431, 1745
Gompertz, B. P., Ravasio, M. E., Nicholl, M., et al. 2023, NatAs, 7, 67
Gottlieb, O., Issa, D., Jacquemin-Ide, J., et al. 2023a, ApJL, 954, L21
Gottlieb, O., Issa, D., Jacquemin-Ide, J., et al. 2023b, ApJL, 953, L11
Gottlieb, O., Jacquemin-Ide, J., Lowell, B., Tchekhovskoy, A., & Ramirez-Ruiz, E. 2023c, ApJL, 952, L32
Gottlieb, O., Lalakos, A., Bromberg, O., Liska, M., & Tchekhovskoy, A. 2022a, MNRAS, 510, 4962
Gottlieb, O., Moseley, S., Ramirez-Aguilar, T., et al. 2022b, ApJL, 933, L2
Gottlieb, O., & Nakar, E. 2022, MNRAS, 517, 1640
Haddadi, M., Duez, M. D., Foucart, F., et al. 2023, CQGra, 40, 085008
Hanauske, M., Takami, K., Bovard, L., et al. 2017, PhRvD, 96, 043004
Hayashi, K., Fujibayashi, S., Kiuchi, K., et al. 2022, PhRvD, 106, 023008
Hayashi, K., Kawaguchi, K., Kiuchi, K., Kyutoku, K., & Shibata, M. 2021, PhRvD, 103, 043007
Hayashi, K., Kiuchi, K., Kyutoku, K., Sekiguchi, Y., & Shibata, M. 2023, PhRvD, 107, 123001
Hjorth, J., Sollerman, J., Møller, P., et al. 2003, Natur, 423, 847
Horesh, A., Hotokezaka, K., Piran, T., Nakar, E., & Hancock, P. 2016, ApJL, 819, L22
Horváth, I., & Tóth, B. G. 2016, Ap&SS, 361, 155
Hotokezaka, K., Kiuchi, K., Kyutoku, K., et al. 2013a, PhRvD, 88, 044026
Hotokezaka, K., Kyutoku, K., Okawa, H., Shibata, M., & Kiuchi, K. 2011, PhRvD, 83, 124008
Hotokezaka, K., Kyutoku, K., Tanaka, M., et al. 2013b, ApJL, 778, L16
Jacquemin-Ide, J., Gottlieb, O., Lowell, B., & Tchekhovskoy, A. 2023, arXiv:2302.07281
Jones, S., Röpke, F. K., Pakmor, R., et al. 2016, A&A, 593, A72
Just, O., Obergaulinger, M., Janka, H. T., Bauswein, A., & Schwarz, N. 2016, ApJL, 816, L30
Kaneko, Y., Bostancı, Z. F., Göğüş, E., & Lin, L. 2015, MNRAS, 452, 824
Kaplan, J. D., Ott, C. D., O'Connor, E. P., et al. 2014, ApJ, 790, 19
Kasen, D., Fernández, R., & Metzger, B. D. 2015, MNRAS, 450, 1777
Kasen, D., Metzger, B., Barnes, J., Quataert, E., & Ramirez-Ruiz, E. 2017, Natur, 551, 80
Kastaun, W., & Galeazzi, F. 2015, PhRvD, 91, 064027
Kawaguchi, K., Kyutoku, K., Nakano, H., et al. 2015, PhRvD, 92, 024014
Kawamura, T., Giacomazzo, B., Kastaun, W., et al. 2016, PhRvD, 94, 064012
King, A., Olsson, E., & Davies, M. B. 2007, MNRAS, 374, L34
Kisaka, S., Ioka, K., & Sakamoto, T. 2017, ApJ, 846, 142
Kiuchi, K., Cerdá-Durán, P., Kyutoku, K., Sekiguchi, Y., & Shibata, M. 2015a, PhRvD, 92, 124034
Kiuchi, K., Kyutoku, K., Sekiguchi, Y., Shibata, M., & Wada, T. 2014, PhRvD, 90, 041502
Kiuchi, K., Reboul-Salze, A., Shibata, M., & Sekiguchi, Y. 2023, arXiv:2306.15721
Kiuchi, K., Sekiguchi, Y., Kyutoku, K., et al. 2015b, PhRvD, 92, 064034
Kiuchi, K., Sekiguchi, Y., Shibata, M., & Taniguchi, K. 2009, PhRvD, 80, 064037
Kiziltan, B., Kottas, A., De Yoreo, M., & Thorsett, S. E. 2013, ApJ, 778, 66

Kluźniak, W., & Ruderman, M. 1998, ApJL, 505, L113
Komissarov, S. S., & Barkov, M. V. 2009, MNRAS, 397, 1153
Kouveliotou, C., Meegan, C. A., Fishman, G. J., et al. 1993, ApJL, 413, L101
Kyutoku, K., Ioka, K., Okawa, H., Shibata, M., & Taniguchi, K. 2015, PhRvD, 92, 044028
Kyutoku, K., Ioka, K., & Shibata, M. 2013, PhRvD, 88, 041503
Kyutoku, K., Okawa, H., Shibata, M., & Taniguchi, K. 2011, PhRvD, 84, 064018
Lamb, G. P., Tanvir, N. R., Levan, A. J., et al. 2019, ApJ, 883, 48
Lattimer, J. M., & Swesty, F. D. 1991, NucPh, A535, 331
Leng, M., & Giannios, D. 2014, MNRAS, 445, L1
Levan, A., Gompertz, B. P., Salafia, O. S., et al. 2023a, arXiv:2307.02098
Levan, A. J., Malesani, D. B., Gompertz, B. P., et al. 2023b, NatAs, 7, 976
Li, L.-X., & Paczyński, B. 1998, ApJL, 507, L59
Lien, A., Sakamoto, T., Barthelmy, S. D., et al. 2016, ApJ, 829, 7
Lippuner, J., Fernández, R., Roberts, L. F., et al. 2017, MNRAS, 472, 904
Liska, M. T. P., Chatterjee, K., Issa, D., et al. 2022, ApJS, 263, 26
Lowell, B., Jacquemin-Ide, J., Tchekhovskoy, A., & Duncan, A. 2023, arXiv:2302.01351
Lü, H.-J., Yuan, H.-Y., Yi, T.-F., et al. 2022, ApJL, 931, L23
Lu, W., & Quataert, E. 2023, MNRAS, 522, 5848
MacFadyen, A. I., & Woosley, S. E. 1999, ApJ, 524, 262
Mahlmann, J. F., Philippov, A. A., Mewes, V., et al. 2023, ApJL, 947, L34
Mangano, V., Holland, S. T., Malesani, D., et al. 2007, A&A, 470, 105
Margalit, B., Jermyn, A. S., Metzger, B. D., Roberts, L. F., & Quataert, E. 2022, ApJ, 939, 51
Margalit, B., & Metzger, B. D. 2017, ApJL, 850, L19
Margalit, B., & Metzger, B. D. 2019, ApJL, 880, L15
Margutti, R., & Chornock, R. 2021, ARA&A, 59, 59
McBreen, B., Hurley, K. J., Long, R., & Metcalfe, L. 1994, MNRAS, 271, 662
McBreen, S., McBreen, B., Hanlon, L., & Quilligan, F. 2002, A&A, 393, L29
Metzger, B. D. 2012, MNRAS, 419, 827
Metzger, B. D., & Bower, G. C. 2014, MNRAS, 437, 1821
Metzger, B. D., & Fernández, R. 2014, MNRAS, 441, 3444
Metzger, B. D., & Fernández, R. 2021, ApJL, 916, L3
Metzger, B. D., Giannios, D., Thompson, T. A., Bucciantini, N., & Quataert, E. 2011, MNRAS, 413, 2031
Metzger, B. D., Martínez-Pinedo, G., Darbha, S., et al. 2010, MNRAS, 406, 2650
Metzger, B. D., Piro, A. L., & Quataert, E. 2008a, MNRAS, 390, 781
Metzger, B. D., Piro, A. L., & Quataert, E. 2009, MNRAS, 396, 1659
Metzger, B. D., Quataert, E., & Thompson, T. A. 2008b, MNRAS, 385, 1455
Metzger, B. D., Thompson, T. A., & Quataert, E. 2018, ApJ, 856, 101
Mooley, K. P., Deller, A. T., Gottlieb, O., et al. 2018, Natur, 561, 355
Most, E. R., & Quataert, E. 2023, ApJL, 947, L15
Mösta, P., Radice, D., Haas, R., Schnetter, E., & Bernuzzi, S. 2020, ApJL, 901, L37
Nagakura, H., Hotokezaka, K., Sekiguchi, Y., Shibata, M., & Ioka, K. 2014, ApJL, 784, L28
Nakar, E. 2007, PhR, 442, 166
Nakar, E. 2020, PhR, 886, 1
Narayan, R., Paczynski, B., & Piran, T. 1992, ApJL, 395, L83
Nomoto, K., & Kondo, Y. 1991, ApJL, 367, L19
Norris, J. P., & Bonnell, J. T. 2006, ApJ, 643, 266
Norris, J. P., & Gehrels, N. 2008, in AIP Conf. Ser. 1000, Gamma-ray Bursts 2007, ed. M. Galassi, D. Palmer, & E. Fenimore (Melville, NY: AIP), 280
Norris, J. P., Gehrels, N., & Scargle, J. D. 2010, ApJ, 717, 411
Özel, F., & Freire, P. 2016, ARA&A, 54, 401
Özel, F., Psaltis, D., Narayan, R., & Santos Villarreal, A. 2012, ApJ, 757, 55
Paczynski, B. 1990, ApJ, 363, 218
Paczynski, B. 1991, AcA, 41, 257
Panaitescu, A. 2011, MNRAS, 414, 1379
Panaitescu, A., & Kumar, P. 2002, ApJ, 571, 779
Paschalidis, V., Ruiz, M., & Shapiro, S. L. 2015, ApJL, 806, L14
Perego, A., Radice, D., & Bernuzzi, S. 2017, ApJL, 850, L37
Perley, D. A., Metzger, B. D., Granot, J., et al. 2009, ApJ, 696, 1871
Popham, R., Woosley, S. E., & Fryer, C. 1999, ApJ, 518, 356
Radice, D., Perego, A., Hotokezaka, K., et al. 2018a, ApJ, 869, 130
Radice, D., Perego, A., Zappa, F., & Bernuzzi, S. 2018b, ApJL, 852, L29
Rantsiou, E., Kobayashi, S., Laguna, P., & Rasio, F. A. 2008, ApJ, 680, 1326
Rastinejad, J. C., Gompertz, B. P., Levan, A. J., et al. 2022, Natur, 612, 223
Rezzolla, L., Baiotti, L., Giacomazzo, B., Link, D., & Font, J. A. 2010, CQGra, 27, 114105
Rezzolla, L., Giacomazzo, B., Baiotti, L., et al. 2011, ApJL, 732, L6
Rezzolla, L., Most, E. R., & Weih, L. R. 2018, ApJL, 852, L25
Rossi, A., Rothberg, B., Palazzi, E., et al. 2022, ApJ, 932, 1
Rosswog, S., Ramirez-Ruiz, E., & Davies, M. B. 2003, MNRAS, 345, 1077
Ruiz, M., Lang, R. N., Paschalidis, V., & Shapiro, S. L. 2016, ApJL, 824, L6
Ruiz, M., Shapiro, S. L., & Tsokaros, A. 2018, PhRvD, 98, 123017
Ruiz, M., Tsokaros, A., & Shapiro, S. L. 2020, PhRvD, 101, 064042
Sarin, N., Lasky, P. D., Vivanco, F. H., et al. 2022, PhRvD, 105, 083004
Schroeder, G., Margalit, B., Fong, W.-f., et al. 2020, ApJ, 902, 82
Schwab, J. 2021, ApJ, 906, 53
Sekiguchi, Y., Kiuchi, K., Kyutoku, K., & Shibata, M. 2011, PhRvL, 107, 051102
Sekiguchi, Y., Kiuchi, K., Kyutoku, K., Shibata, M., & Taniguchi, K. 2016, PhRvD, 93, 124046
Shibata, M., Duez, M. D., Liu, Y. T., Shapiro, S. L., & Stephens, B. C. 2006, PhRvL, 96, 031102
Shibata, M., Fujibayashi, S., Hotokezaka, K., et al. 2017, PhRvD, 96, 123012
Shibata, M., & Hotokezaka, K. 2019, ARNPS, 69, 41
Shibata, M., & Taniguchi, K. 2006, PhRvD, 73, 064027
Shibata, M., & Taniguchi, K. 2008, PhRvD, 77, 084015
Shibata, M., & Taniguchi, K. 2011, LRR, 14, 6
Shibata, M., & Uryū, K. 2006, PhRvD, 74, 121503
Shibata, M., & Uryū, K. 2007, CQGra, 24, S125
Siegel, D. M., & Metzger, B. D. 2017, PhRvL, 119, 231102
Siegel, D. M., & Metzger, B. D. 2018, ApJ, 858, 52
SpEC collaboration 2023, Spectral Einstein Code, https://www.black-holes.org/code/SpEC
Stanbro, M., & Meegan, C. 2016, GCN, 19843, 1
Steiner, A. W., Hempel, M., & Fischer, T. 2013, ApJ, 774, 17
Sun, H., Wang, C. W., Yang, J., et al. 2023, arXiv:2307.05689
Sun, L., Ruiz, M., Shapiro, S. L., & Tsokaros, A. 2022, PhRvD, 105, 104028
Svinkin, D., Frederiks, D., Ridnaia, A., et al. 2023, GCN, 33579, 1
Taam, R. E., & van den Heuvel, E. P. J. 1986, ApJ, 305, 235
Tamura, T., Yoshida, A., Sakamoto, T., et al. 2021, GCN, 31226, 1
Tanvir, N. R., Levan, A. J., Fruchter, A. S., et al. 2013, Natur, 500, 547
Tarnopolski, M. 2016, MNRAS, 458, 2024
Tauris, T. M., Kramer, M., Freire, P. C. C., et al. 2017, ApJ, 846, 170
Tchekhovskoy, A. 2015, in The Formation and Disruption of Black Hole Jets, ed. I. Contopoulos, D. Gabuzda, & N. Kylafis, 414 (Berlin: Springer), 45
Tchekhovskoy, A., Narayan, R., & McKinney, J. C. 2011, MNRAS, 418, L79
Thompson, C. 1994, MNRAS, 270, 480
Thompson, T. A., Burrows, A., & Meyer, B. S. 2001, ApJ, 562, 887
Thompson, T. A., Chang, P., & Quataert, E. 2004, ApJ, 611, 380
Troja, E., Fryer, C. L., O'Connor, B., et al. 2022, Natur, 612, 228
Usov, V. V. 1992, Natur, 357, 472
Vigna-Gómez, A., Neijssel, C. J., Stevenson, S., et al. 2018, MNRAS, 481, 4009
Woosley, S. E. 1993, ApJ, 405, 273
Xiao, S., Zhang, Y.-Q., Zhu, Z.-P., et al. 2022, arXiv:2205.02186
Yang, J., Ai, S., Zhang, B.-B., et al. 2022, Natur, 612, 232
Yang, Y.-H., Troja, E., O'Connor, B., et al. 2023, arXiv:2308.00638
Yin, Y.-H. I., Zhang, B.-B., Sun, H., et al. 2023, ApJL, 954, L17
Yoon, S. C., Podsiadlowski, P., & Rosswog, S. 2007, MNRAS, 380, 933
Zhang, B., & Mészáros, P. 2001, ApJL, 552, L35
Zhang, H.-M., Huang, Y.-Y., Zheng, J.-H., Liu, R.-Y., & Wang, X.-Y. 2022, ApJL, 933, L22
Zhu, J.-P., Wang, X. I., Sun, H., et al. 2022, ApJL, 936, L10